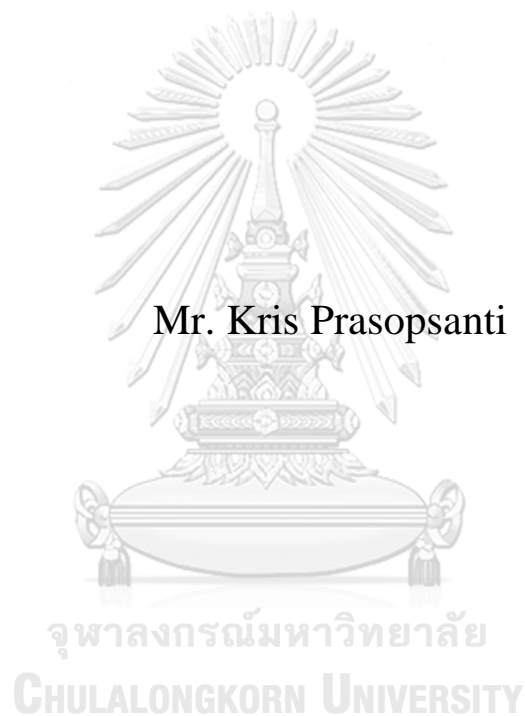


DESIGN OF PLANTWIDE CONTROL STRUCTURE OF
DOUBLE EFFECT WATER/LITHIUM BROMIDE
ABSORPTION CHILLER



A Thesis Submitted in Partial Fulfillment of the Requirements
for the Degree of Master of Engineering in Chemical Engineering
Department of Chemical Engineering
Faculty of Engineering
Chulalongkorn University
Academic Year 2018
Copyright of Chulalongkorn University

การออกแบบโครงสร้างการควบคุมแบบเฟลนที่ไว้ค้ของระบบทำความเย็นแบบดูดซึม
ด้วยน้ำ/ลิเทียมโบรไมด์ชนิดสองชั้น



วิทยานิพนธ์นี้เป็นส่วนหนึ่งของการศึกษาตามหลักสูตรปริญญาวิศวกรรมศาสตรมหาบัณฑิต
สาขาวิชาวิศวกรรมเคมี ภาควิชาวิศวกรรมเคมี
คณะวิศวกรรมศาสตร์ จุฬาลงกรณ์มหาวิทยาลัย
ปีการศึกษา 2561
ลิขสิทธิ์ของจุฬาลงกรณ์มหาวิทยาลัย

Thesis Title DESIGN OF PLANTWIDE CONTROL STRUCTURE
OF DOUBLE EFFECT WATER/LITHIUM BROMID
E ABSORPTION CHILLER
By Mr. Kris Prasopsanti
Field of Study Chemical Engineering
Thesis Advisor Professor Paisan Kittisupakorn, Ph.D.

Accepted by the Faculty of Engineering, Chulalongkorn University in Partial
Fulfillment of the Requirement for the Master of Engineering

..... Dean of the Faculty of Engineering
(Associate Professor Supot Teachavorasinskun, D.Eng.)

THESIS COMMITTEE

..... Chairman
(Varun Taepaisitphongse, Ph.D.)
..... Thesis Advisor
(Professor Paisan Kittisupakorn, Ph.D.)
..... Examiner
(Associate Professor Tharathon Mongkhonsi, Ph.D.)
..... External Examiner
(Assistant Professor Wachira Daosud, D.Eng.)


จุฬาลงกรณ์มหาวิทยาลัย
CHULALONGKORN UNIVERSITY

กฤษฎี ประสพสันติ : การออกแบบโครงสร้างการควบคุมแบบแพลนที่ไวด์ของระบบทำความเย็นแบบดูดซึม ด้วย
น้ำ/ลิเทียมโบรไมด์ชนิดสองชั้น. (

DESIGN OF PLANTWIDE CONTROL STRUCTURE OF DOUBLE EF
FECT WATER/LITHIUM BROMIDE ABSORPTION CHILLER) อ.ที่

ปรึกษาหลัก : ศ. ดร.ไพศาล กิตติศุภกร

งานวิจัยนี้ นำเสนอการออกแบบโครงสร้างการแบบแพลนที่ไวด์ของระบบทำความเย็น
แบบดูดซึมด้วยน้ำ/ลิเทียมโบรไมด์ชนิดสองชั้น ด้วยวิธีการของ Skogastad
ภายใต้แผนการดำเนินงานสองลักษณะ สำหรับการดำเนินงานแบบกำหนดอัตราการผลิต ระบบการควบคุมแบบแยกจากศูนย์
(Decentralized) สองโครงสร้างและระบบควบคุมแบบโมเดลพรีดิกทีฟ ได้ถูกนำเสนอและเปรียบเทียบโดยใช้การจำลอง
กระบวนการด้วยโปรแกรมแมตแล็บ-ซิมูลิงค์ (MATLAB-Simulink) โดยเมื่อเปรียบเทียบกันแล้วประสิทธิภาพใน
การจัดการกับตัวแปรบกวนของแต่ละระบบการควบคุมนั้นแตกต่างกันไปตามประเภทของตัวแปรบกวน แต่โดยภาพรวม
ระบบควบคุมแบบโมเดลพรีดิกทีฟควบคุมระบบได้ดีกว่าระบบการควบคุมแบบแยกจากศูนย์ โดยระบบดังกล่าวสามารถควบคุม
การสะสมของมวลดีกว่าและใช้เวลาในการเข้าสู่สภาวะใหม่ได้เร็วกว่าโดยเฉลี่ย สำหรับการดำเนินงานด้วยแบบกำหนดอัตราการ
ป้อนคงที่ หลักการควบคุมโดยการหาค่าเหมาะที่สุดด้วยตนเอง (Self-Optimizing Control) ได้ถูกนำมาประยุกต์ใช้
โดยวิธีการ ค่าเอกฐานต่ำสุด (Minimum Singular Value, MSV) และ ปริภูมิศูนย์ (Null Space) เพื่อหา
ตัวแปรควบคุมที่เหมาะสม โดยผลลัพธ์จากทั้งสองวิธีสามารถลดการสูญเสียประสิทธิภาพส่วนใหญ่เมื่อระบบถูกรบกวนลง
ได้ โดยตัวแปรจากวิธีปริภูมิศูนย์มีประสิทธิผลดีกว่าเล็กน้อยในกรณีที่อุณหภูมิของน้ำหล่อเย็นและอัตราการให้ความร้อนเข้าสู่
ระบบซึ่งเป็นตัวแปรบกวนหลักมีการเปลี่ยนแปลง

จุฬาลงกรณ์มหาวิทยาลัย
CHULALONGKORN UNIVERSITY

สาขาวิชา วิศวกรรมเคมี
ปีการศึกษา 2561

ลายมือชื่อนิสิต
ลายมือชื่อ อ.ที่ปรึกษาหลัก

5770539521 : MAJOR CHEMICAL ENGINEERING

KEYWORD Absorption chiller, Control structure design, Plantwide control

D:

Kris Prasopsanti :
 DESIGN OF PLANTWIDE CONTROL STRUCTURE OF DOUBLE EFFECT WATER/LITHIUM BROMIDE ABSORPTION CHILLER.
 Advisor: Prof. Paisan Kittisupakorn, Ph.D.

Alternative control structures for a parallel double effect aqueous lithium bromide absorption chiller, operated in two modes of operation, has been designed using Skogastad's plantwide control procedure. In on-demand mode, two complete decentralized control structures with proportional integral (PI) controllers and one structure with a two inputs – two outputs model predictive controller (MPC) were proposed. Their performance was evaluated using MATLAB-Simulink dynamic simulation. The results varied depended on type of disturbance, but overall, the structure with MPC controller provided slightly better results with less liquid holdup changes and faster setting time in average. For on-supply mode, two self-optimizing control variables obtained from minimum singular value (MSV) and null space method were implemented to a decentralized control structure. In general, both variables were able to reduce majority of loss due to change in optimal process conditions. Nevertheless, the null space control variable provided slightly better results for main disturbances, which are cooling utility temperature and amount of heat input.



Field of Study: Chemical Engineering

Student's Signature

Academic Year: 2018

Advisor's Signature

Year:

.....

ACKNOWLEDGEMENTS

First, I would like to express my great appreciation to my thesis supervisor, Professor Paisan Kittisupakorn for the great opportunity, inspiration, and kind supporting. I am also very grateful to be part of a supporting research facility at Control and System Engineering Research Laboratory in the Department of Chemical Engineering, Engineering Faculty, Chulalongkorn University.

Kris Prasopsanti



TABLE OF CONTENTS

	Page
ABSTRACT (THAI)	iii
ABSTRACT (ENGLISH).....	iv
ACKNOWLEDGEMENTS.....	v
TABLE OF CONTENTS.....	vi
LIST OF FIGURES	vii
LIST OF TABLES.....	x
NOMENCLATURES	xii
CHAPTER I INTRODUCTION.....	1
1.1 Background and Motivation.....	1
1.2 Research Objectives.....	3
1.3 Scopes of Work.....	3
CHAPTER II LITERATURE REVIEWS	4
2.1 Absorption Chiller Dynamic Simulation.....	4
2.2 Absorption Chiller Control.....	5
2.3 Plantwide Control.....	5
CHAPTER III THEORY.....	9
3.1 Absorption Chiller	9
3.1.1. Water/lithium bromide Solution.....	11
3.1.2. Single Effect Water/lithium bromide Absorption Chillers.....	15
3.1.3. Double Effect Water/lithium bromide Absorption Chillers	16
3.1.4. Heat Exchanger	17
3.2 Plantwide Control Strategy.....	18
3.2.1. Define the Operational Objectives	20
3.2.2. Selection of Manipulated Variables, Degree of Freedom Analysis and Steady State Optimization	20
3.2.3. Select Primary (economic) Controlled Variables.....	21

3.2.4. Set the Throughput Manipulator (TPM) Location	24
3.2.5. Bottom Up Control Structure Design	24
CHAPTER IV ABSORPTION CHILLER PROCESS CHARACTERISTIC AND DESIGN	29
4.1 Absorption Chiller Models	29
4.2 Mathematical Model Validation	31
CHAPTER V TOP-DOWN PLANTWIDE CONTROL	35
5.1 Define Operational Objective	35
5.2 Optimize Process Nominal Operating Conditions	36
5.3 Select Primary Controlled Variables	38
5.3.1 Minimum Singular Value	38
5.3.2 Null-Space Method	47
5.4 Location of Throughput Manipulator	48
CHAPTER VI BOTTOM-UP STRUCTURE DESIGN	49
Pressure and Temperature Control	49
6.1 On-Demand Mode of Operation	49
6.2 On-Supply Mode of Operation	62
CHAPTER VII CONCLUSIONS	69
REFERENCES	70
APPENDIX	73
A.1 System Identification	73
A.2 PI Controller Tuning	74
B.1 Transfer Functions	75
B.2 Controller Parameters	76
VITA	77

LIST OF FIGURES

	Pages
Figure 3.1 A vapor-compression refrigeration cycle	9
Figure 3.2 Combination between a vapor-compression refrigerator and power generator	10
Figure 3.3 Water/lithium bromide phase diagram	12
Figure 3.4 Water/lithium bromide Dühring's chart	13
Figure 3.5 Enthalpy–mass fraction diagram	14
Figure 3.6 A single effect chiller	15
Figure 3.7 A parallel flow double effect chiller	16
Figure 3.8 Dühring state plot for a parallel flow chiller	16
Figure 3.9 Plant horizontal decomposition diagram	19
Figure 3.10 Loss incurred by keeping constant setpoint for different control variables	22
Figure 3.11 MPC concept	25
Figure 3.12 PID model	28
Figure 4.1 A parallel flow double effect chiller	32
Figure 4.2 COP as a function of temperature in a high-pressure generator	32
Figure 4.3 Comparison of simulation results and data from Khan <i>et al.</i> (2017)	32
Figure 4.4 Comparison of simulation results and data from Dixit (2016)	33
Figure 5.1 COP as a function of splitting ratio at nominal operating condition	37
Figure 5.2 COP as a function of a low-pressure condenser temperature	37
Figure 5.3 COP as a function of splitting ratio as T_{c1} changed by $\pm 2^\circ\text{C}$	39
Figure 5.4 COP as a function of splitting ratio as Q_{g2} changed by $\pm 10\%$	40
Figure 5.5 COP as a function of splitting ratio as T_e changed by $\pm 2^\circ\text{C}$	42
Figure 5.6 COP as a function of splitting ratio as T_{g2} changed by $\pm 5^\circ\text{C}$	43
Figure 5.7 COP loss estimation as T_{c1} changed by $\pm 2^\circ\text{C}$	45

Figure 5.8 COP loss estimation as Q_{g2} changed by $\pm 10\%$	46
Figure 5.9 COP loss estimation as T_e changed by $\pm 2^\circ\text{C}$	47
Figure 5.10 COP loss estimation as T_{g2} changed by $\pm 5^\circ\text{C}$	47
Figure 6.1 PID1 structure.....	51
Figure 6.2 PID2 structure.....	51
Figure 6.3 MPC structure.....	51
Figure 6.4a Heat input as T_{c1} changed by $\pm 2^\circ\text{C}$	53
Figure 6.4b Level in C1 as T_{c1} changed by $\pm 2^\circ\text{C}$	53
Figure 6.4c Level in C2 as T_{c1} changed by $\pm 2^\circ\text{C}$	53
Figure 6.4d LiBr mass fraction as T_{c1} increased by 2°C	53
Figure 6.5a Heat input as production rate changed by $\pm 10\%$	57
Figure 6.5b Level C1 in as production rate changed by $\pm 10\%$	57
Figure 6.5c Level C2 in as production rate changed by $\pm 10\%$	57
Figure 6.5d LiBr mass fraction as production rate increased by $\pm 10\%$	57
Figure 6.6a Heat input as T_e changed by $\pm 2^\circ\text{C}$	58
Figure 6.6b Level in C1 as T_e changed by $\pm 2^\circ\text{C}$	58
Figure 6.6c Level in C2 as T_e changed by $\pm 2^\circ\text{C}$	58
Figure 6.6d LiBr mass fraction T_e reduced by 2°C	58
Figure 6.7a Heat input as T_{g2} changed by $\pm 5^\circ\text{C}$	59
Figure 6.7b Level in C1 as T_{g2} changed by $\pm 5^\circ\text{C}$	59
Figure 6.7c Level C2 in as T_{g2} changed by $\pm 5^\circ\text{C}$	59
Figure 6.7d LiBr mass fraction as T_{g2} reduced by 5°C	59
Figure 6.8 DRGA.....	60
Figure 6.9a Heat input as T_{c1} decreased by 2°C	61
Figure 6.9b Level in C2 as T_{c1} decreased by 2°C	61
Figure 6.9c Level in C1 as T_{c1} decreases by 2°C	62
Figure 6.9d Level in G2 as T_{c1} decreased by 2°C	62
Figure 6.10 PID 3 structure.....	63
Figure 6.11 COP for each structure as T_{c1} changed by 2°C	65

Figure 6.12 COP for each structure as Q_{g2} changed by 10%	66
Figure 6.13 COP for each structure as T_e changed by 2°C.....	67
Figure 6.14 COP for each structure as T_{g2} changed by 5°C.....	68
Figure A.1 Step response experiment	73



LIST OF TABLES

	Pages
Table 3.1 Comparison between water/lithium bromide and ammonia/water solution	10
Table 3.2 Meaning of the value of λ_{ij}	27
Table 4.1 Comparison of major energy transfer between simulation results and data from Herold <i>et al.</i> (2016)	31
Table 4.2 Design specifications	34
Table 5.1 CDOF of a double effect absorption	36
Table 5.2 Gain value of control variable candidates	38
Table 5.3 MSV index of control variable candidates as T_{c1} changed by $\pm 2^\circ\text{C}$	40
Table 5.4 MSV index of control variable candidates as Q_{g2} changed by $\pm 10\%$	41
Table 5.5 MSV index of control variable candidates as T_e changed by $\pm 2^\circ\text{C}$	43
Table 5.6 MSV index of control variable candidates as T_{g2} changed by $\pm 5^\circ\text{C}$	44
Table 5.7 Overall MSV index of control variable candidates.....	45
Table 5.8 Loss reduction as P_2 was used as a control variable	47
Table 6.1 input-output for liquid holdup control.....	50
Table 6.2 RGA values for liquid holdup control.....	50
Table 6.3 Comparison of performance indices as T_{c1} decreased by 2°C	52
Table 6.4 Comparison of performance indices as T_{c1} increased by 2°C	52
Table 6.5 Comparison of performance indices as production rate increased by 10% 54	54
Table 6.6 Comparison of performance indices as production rate decreased by 10% 54	54
Table 6.7 Comparison of performance indices as T_e decreased by 2°C	55
Table 6.8 Comparison of performance indices as T_e increased by 2°C	55
Table 6.9 Comparison of performance indices as T_{g2} decreased by 5°C	55
Table 6.10 Comparison of performance indices as T_{g2} increased by 5°C	56
Table 6.11 MPC structure comparison as T_{c1} decreased by 2°C	61
Table 6.12 RGA values for liquid holdup control in on-supply mode.....	62

Table 6.13 COP at the worst cases of disturbance	64
Table B.1.1 Transfer functions for liquid holdup control	75
Table B.2.1 PI Controller parameters.....	76
Table B.2.2 MPC Controller parameters.....	76



NOMENCLATURES

<i>A</i>	Area (m ²)
<i>C_p</i>	Heat capacity (kJ kg ⁻¹ / °C)
<i>C_v</i>	Flow coefficient
CDOF	Control degree of freedom
<i>C_m</i>	Control valve coefficient (kg ^{0.5} /min)
COP	Coefficient of performance
CV	Controlled variable
<i>d</i>	Disturbance
<i>G</i>	Gain
<i>h</i>	Specific Entropy (kJ/kg)
<i>J</i>	Cost function
<i>L</i>	Loss function
<i>M</i>	Liquid holdup (kg)
<i>m</i>	Mass flow rate (kg/min)
<i>N_{m0}</i>	Number of manipulated inputs with no steady state effect
<i>N_{ss}</i>	Steady-state degree of freedom
<i>N_{y0}</i>	Control variables with no steady-state effect
<i>P</i>	Pressure
<i>P₀</i>	Pressure in an evaporator (MPa)
<i>P₁</i>	Pressure in a low-pressure condenser (MPa)
<i>P₂</i>	Pressure in a high-pressure condenser (MPa)
<i>Q</i>	Energy flow rate (kJ/min)

R	Splitting ratio
S_i	Scale matrix
T	Temperature ($^{\circ}\text{C}$)
TPM	Throughput manipulator
U	Heat transfer coefficient ($\text{kJ}/(^{\circ}\text{C} \cdot \text{min} \cdot \text{m}^2)$)
u	Manipulated variable
W	Work (kJ/min)
x	LiBr mass fraction (kg/kg)
z	Control variable candidate
ϵ	Heat transfer effectiveness
λ	Relative gain
θ	Time delay (min)
ω	frequency (min^{-1})

Unit

a	Absorber
c1	Low-pressure condenser
c2	High-pressure condenser
e	Evaporator
g1	Low-pressure generator
g2	High-pressure generator

CHAPTER I

INTRODUCTION

1.1 Background and Motivation

Process control structure duties are ensured the safety and satisfactory process conditions such as smooth operate as well as disturbance rejection and optimizing process performance. For decades, chemical industries have been utilizing the “unit operations approach” to design the said structure (Stephanopoulos, 1983). The approach starts with decomposing of the process into individual units, then a control system is designed for each unit separately. Thereby, the final structure is just a combination of those individual systems. This is a well-established method that benefits from many tools developed along the industry history. However, the main assumption of the method is the whole process behaves as a summation of its individual parts and any conflicts among the control loops as well as interactions between the units altogether are ignored. Whereas the approach can establish the effective control schemes for individual units, it is not proper for the complex processes with high degree of interaction such as processes with many materials recycles or complex heat transfer integration. As, for those processes, an output of a unit acts as a disturbance for others (Larsson & Skogestad, 2000) which should be considered in order to design high performance control structures.

One of the most famous words described the basic idea of plantwide control was stated by Foss (1973) as follow “The central issue to be resolved by the new theories is the determination of the control system structure. Which variables should be measured, which inputs should be manipulated, and which links should be made between the two sets? [...], for without it the control configuration problem will likely remain in primitive, hazily stated and wholly unmanageable form. The gap is present indeed, but contrary to the views of many, it is the theoretician who must close it”. Basically, the main focus of the control structure design is to answer three questions; which measurements should be controlled, which input should be used, and which kind of controller should be utilized to connect the two sets.

A plantwide control structure design can be defined as a set of methods to design control structures for the whole plant. While the essential idea is to answer the three questions stated by Foss, there are many approaches and alternative strategies proposed over last two decades (Rangaiah & Kariwala, 2012). Furthermore, depend on perspective, there is no unique “correct” or the most effective approach.

There are two groups of plantwide control strategy; heuristics-based approaches such as Luyben’s (1997) and Wongsri’s (2006), and algorithmic-based approaches such as McAvoy’s (1994). Since a double effect absorption chiller, the process used as case study, is rather simple compared to an entire chemical plant with dozens or hundreds manipulated variables and measurements, pure heuristics-based approaches which depend on process insight and rules established from experience, cannot be fully utilized (Larsson & Skogestad, 2000). Wherefore, the approach used in this study is Skogestad’s plantwide control strategy (Skogestad, 2004). The approach is a hybrid of heuristic and algorithmic method as it adopts many of Luyben’s basic concepts such as plant objective and throughput manipulator location, and at the same time utilizes mathematic tools such as minimum singular gain to determine its optimal control structures. The method is also referred as economic plantwide control as it is much more focused on economic objective with the concept of self-optimizing compared to Luyben’s emphasis on stability.

As aforementioned, the process studied in this work was a double effect absorption chiller. The chiller is one of the oldest cooling technologies and have been used for ice production processes since mid-1700s way before vapor compression systems were introduced in 1970s. Despite the age of technology, in late decades, the usage of the absorption chiller in the industries and public infrastructures had been dramatically increasing because of three main reasons.

The first reason was the rising concern about energy conservation in industries and government. In such wise, more heat transfer integrations are implemented to the processes resulted in increasing demand of the cooling technologies. The second reason was the escalating of electricity price as well as the limited usage of chlorofluorocarbon (CFC) which made an absorption chiller become more competitive compared to vapor compression systems, as the system could use waste heat from other processes as its source of energy and generally used more

environmentally friendly solution such as aqua lithium bromide and ammonia as refrigerant. The last reason was the promoting of renewable energy utilization as an absorption chiller technology, especially when aqua lithium bromide was used as the refrigerant, was able to use solar energy as its main energy source. Despite all the positive, its high capital costs of equipment as well as low energy efficiency compared to a vapor compression chiller still limited the usage of the system. Nevertheless, future of the technology was promising.

Consequently, the dynamic behavior of a 100 USRT (352 kW) parallel flow double effect aqueous lithium bromide chiller was used as a case study. The system was simulated in two modes of operation by Matlab-Simulink program. For on-demand mode of operation, three promising control structures were designed and analyzed. And the main concept of Skogastad's plantwide control strategy, the self-optimizing control, was applied on the system operated in on-supply mode of operation.

1.2 Research Objectives

The objective of this research is to design control structures for a parallel flow double effect water/lithium bromide absorption chiller to achieve high effectiveness.

1.3 Scopes of Work

1.3.1 Modeling and simulating a 100 USRT parallel flow double effect water/lithium bromide absorption chiller with 0.7 MPa saturated steam as heat source in two mode of operation using MATLAB-Simulink.

1.3.2 Design and simulating alternative control structures based on Skogestad's plantwide control procedure (2012).

1.3.3 Comparing three proposed regulatory control structures in the on-demand mode of operation.

1.3.4 Evaluating effect of self-optimizing control variables in the on-supply mode of operation.

CHAPTER II

LITERATURE REVIEWS

In this chapter, the literature reviews were divided into three parts; (i) an overview of research regarding absorption chiller dynamic simulation, (ii) absorption chiller control and (iii) plantwide control procedure.

2.1 Absorption Chiller Dynamic Simulation

There were several notable studies about the dynamic model of a single effect water/lithium bromide chiller. First, Jeong *et al.* (1998) proposed a dynamic simulation of a single effect chiller using the waste heat. Simple dynamic concepts of mass balance, energy balance and vapor pressure were used to generate the model. In absorber and generator, a homogenous thermal equilibrium state was assumed, and thermodynamic states were also considered as constant throughout all equipment. The effects of the temperature, the mass flow rate of the heat sink, the heat transfer area of the system components and the working fluid circulation rate on the system performance were investigated. But only the exchanged heat in key component was used for the model verification and the simulation result agreed with the experimental data.

Kohlenbach and Ziegler (2008) proposed a simple model based on external and internal steady-state enthalpy balances for each main component. Only storage and time delay term were used to represent the dynamic behaviors and temperature-dependent parameters were assumed constant. The model predicted the transiency of the chiller well with deviations of ten second compared to the experiment data. However, the exact values did not match. In 2015, Lazrak *et al.* (2016) proposed a dynamic artificial neural network, a black box model of a single effect absorption chiller. So, the model worked reasonably well as it was able to predict outlet temperature and the transferred energy with the range of 1.1 - 5% and 1 - 6% of errors, respectively.

Xu *et al.* (2016) proposed a model applying Nusselt solution for film thickness and velocity distribution on a horizontal tube in the absorber. The model had relative

error less than 5% in all key parameters while the step change temperature of heat input by 10°C.

There were less studies on double effect chillers, however. Shin *et al.* (2009) proposed a dynamic using valve throttling and 'U' tube to model mass transport mechanisms among the main components. The model used dynamic equations to find thermodynamic properties of working fluid via numerical methods. It showed a good agreement with the test data except for the first 83 minutes after start-up.

2.2 Absorption Chiller Control

In the present, some research mentioned about chiller control strategies. Shin *et al.* (2009) applied a simple proportional controller to a double effect chiller. The step change of the load from 100% to 20% was tested and the controller took around 15-20 minutes to stabilize the chiller into new set points. This similar delay was also reported in Kohlenbach and Ziegler (2008) work. Seo *et al.* (2012) developed control of levels in high temperature generator by using level switches. As a result, the switches could reduce the charging amount of the solution and improve controllability.

Recently, there is some research studied on effect of a generator temperature. Fernández-Seara and Vázquez (2001) studied on the optimal generator temperature in a single effect chiller to maximize the coefficient of performance. The simple on-off control and PID control were proposed to maintain the optimal temperature by varying the heat input. Rêgo *et al.* (2014) also claimed that this approach provided a better performance than the chilled water temperature control. The idea of generator temperature control was applied to a parallel double effect chiller by Dixit (2016). In their research, steady state analysis was performed to determine the optimal splitting ratio while temperature in an evaporator, a low-pressure condenser and a high-pressure generator were varied.

2.3 Plantwide Control

The concept of the plantwide control was first introduced by Buckley (1964). In his book, he separated the problem in to two parts depending on frequency of

disturbances; material balance and product quality control. He suggested dealing with low-frequency disturbances inventory control via material balance first and then quality control with high-frequency disturbances later. The main idea was, as speed of the quality control was in an order of magnitude higher than that of material balance control, the states in material balance could be treated as pseudo steady-states and the two structure would have no interaction. There were also discussions about many issues such as production rate control, indirect control, predictive optimization, recycle and the need of purge inert. In general, the study presented many ideas that are the principles of the plantwide control but did not provide any procedure. Despite this first study was presented as early as 1964, most of the developments have not occurred until the last two decades.

The first systematic procedure was proposed by Govind and Powers (1982). It was a heuristics-based procedure providing set of control rules based on simple model to design new control structures as well as methods to select the manipulated variables. Narraway and Perkins (1993) used Mixed-Integer Nonlinear Programming (MINLP) optimization techniques to evaluate the controllability and select the control structure. Whereas the method was reasonable mathematically, the brute force optimization required a large resource of computer processing and could not be used for a large and a complex process. A more practical numerical approach was presented by T. J. McAvoy and Ye (1994). They used the Bukley's concept of the decomposition based on the control speed and divided the control structure into four stages; flow, level, pressure and composition. In their procedure, mathematical tools such as relative gain array, Niederlinski index and disturbance analysis were utilized. It also involved higher-level control such as model predictive control. In the same year, Wolff *et al.* (1994) proposed a plantwide control strategy with emphasizing on the process-oriented decomposition approaches. They suggested that plantwide control system design should start with a "top-down" selection of controlled and manipulated variables and one proceed with a "bottom-up" design of the control system. At the end of the paper ten heuristic guidelines for plantwide control were listed.

The first complete plantwide control procedure was proposed by Luyben *et al.* (1997). It was made to correct three flaws in Bukley's approach including with no

energy management, discussion about the recycles and placed the emphasis on the inventory rather than the quality control. Luyben's approach was a nine steps heuristics-based procedure that could generate the entire control structure for a plant. Those steps included; establishing control objectives, determining the degree of freedom, energy management system, production rate and product quality control as well as handle the safety, inventories control, check component balance, design control system for each individual unit, and economic optimization or improve controllability. The procedure had served as the framework of many following plantwide control procedures such as Skogestad's (2004), Konda's (2005) and Wongsri's (2006). The approach was demonstrated on Tennessee Eastman, hydrodealkylation of toluene (HDA) and vinyl acetate monomer (VAM) plants.

Nevertheless, the main weakness of Luyben's procedure was it did not emphasize enough on economic as it only includes economic optimization as an optional in the last step, so the control structure resulted may perform poorly economical wise (Larsson & Skogestad, 2000).

Zheng *et al.* (1999) proposed a hierarchical procedure that decomposition the control problem into a hierarchy of decisions based on process economics including steady-state robust feasibility, selection of controlled variables, steady-state control structure screening, dynamic control structure synthesis, Economic ranking and dynamic simulation. The main advantage of this hierarchical method is it solved one part of the problem at a time instead of one large complex problem.

In 2004, an economical centric procedure utilized the idea of self-optimizing control was proposed by Skogestad. The main concept of "self-optimizing control" was first introduced by Morari (1980). As in his paper, the concept of finding a function of the process variables which when held constant, led automatically to the optimal adjustments of the manipulated variables was mentioned. However, it did not get much attention at the time. Skogestad and Postlethwaite (1996) presented the mathematical approach to find self-optimizing control variables using the minimum singular value of the gain matrix and, the concept of self-optimizing control was defined by Skogastad (2000). The concept is almost identical to Morari's idea except the term "optimal adjustment" was replaced by "acceptable adjustment". He also gave four qualitative requirements of the preferred control variables.

Konda et al. (2005) proposed an eight-steps improved heuristic methodology based on Luyben's procedure integrated with the simulation to overcome the overreliance on the experience in purely heuristics-based methods. Zhang *et al.* (2010) compared performance of the last two methodologies for ammonia synthesis process. While Konda's control structure performed better in terms of control and management of production rate during the transient period, Skogastad's structure gave higher normalized profit.



CHAPTER III

THEORY

This chapter was divided into two parts; (i) principle of absorption chillers, (ii) Skogestad's plantwide control procedure.

3.1 Absorption Chiller

An absorption chiller is one of the heat pump technologies, which is a group of technologies that transfer heat from low temperature to high temperature. According to the thermodynamic second law, this kind of transfer requires external work input to make it possible. For instance, in case of a vapor-compression refrigeration cycle, work input from a compressor is used to generate the pressure difference between the two states.

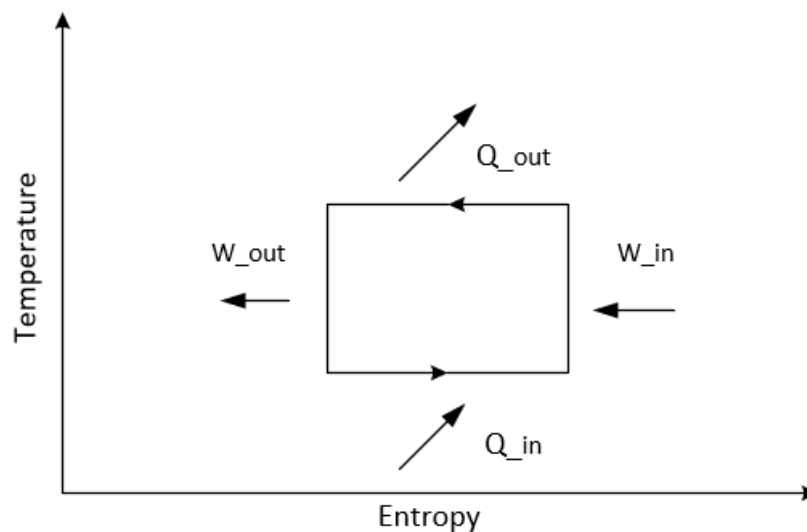


Figure 3.1 A vapor-compression refrigeration cycle (Smith *et al.*, 2005)

Basically, a single effect absorption chiller can be described as a combination of the vapor-compression refrigerator and power generator system as shown in Figure 3.2. This configuration eliminates the need of vapor compressor as well as majority of work input added to the system. However, condense the vapor from the evaporator back to the liquid using a condenser is not practical, so a solvent is introduced and a condenser and a boiler on the power generator side are replaced with an absorber and a generator, respectively.

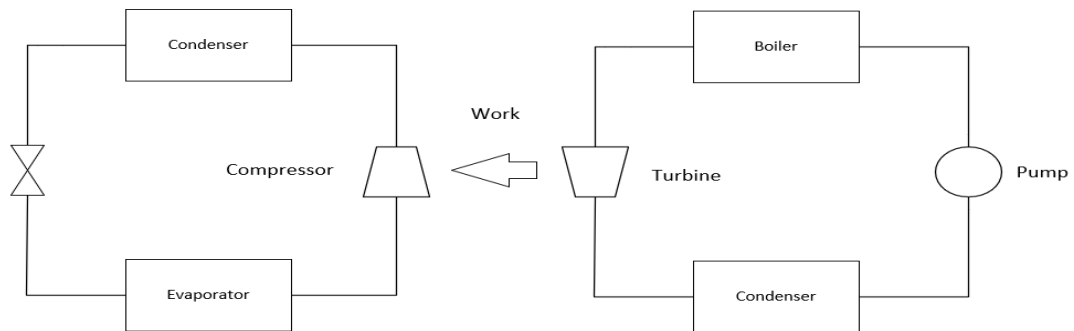


Figure 3.2 Combination between a vapor-compression refrigerator and power generator (Smith *et al.*, 2005)

For the choice of the mixture, currently, water/lithium bromide and ammonia/water are two prominent solutions used in an absorption chiller as they provided most desirable properties compared to other alternatives (Herold *et al.*, 2016). Both have their own advantages and disadvantages as listed in Table 3.1.

Table 3.1 Comparison between water/lithium bromide and ammonia/water solution (Herold *et al.*, 2016)

Property	Ammonia/Water	Water/Lithium Bromide
Refrigerant		
High latent heat	Good	Excellent
Moderate vapor pressure	Too high	Too low
Low freezing temperature	Excellent	Limited application
Low viscosity	Good	Good
Absorbent		
Low vapor pressure	Poor	Excellent
Low viscosity	Good	Good
Mixture		
No solid phase	Excellent	Limit application
Low toxicity	Poor	Good
High affinity between refrigerant and absorbent	Good	Good

Whereas water/lithium bromide chillers have been the most commonly used chiller type since they were pioneered in 1930s (Berestneff, 1949), the main downside is the working fluid high crystallization temperature, as solidified solution can result in interruption of machine operation and possible damage the unit. The usage of water as refrigerant also limits the range of chiller applications since its minimum refrigeration temperature is relatively high compared to ammonia or other commercial refrigerants.

On the other hand, ammonia/water chiller is an older technology as the technology has been used since 1800s. The strong point of the technology is freezing temperature of ammonia which is -77.7°C . However, the major drawback is the toxicity of the refringence. Moreover, it is less suit for solar energy as ammonia/water is characterized by an average 10–15% lower solar fraction than water/lithium bromide (Li & Sumathy, 2000).

3.1.1. Water/lithium bromide Solution

The main disadvantage of water/lithium bromide mixture is the risk of crystallization. As a salt solution, a solid hydrate phase of lithium bromide is precipitated when the mass fraction is exceeded the solution limit. This limit has strong relation with both mass fraction of lithium bromide and temperature and weak relation with pressure. The phase diagram of aqueous lithium bromide solution is shown in Figure 3.3 and the limit can be estimated by Eq 3.1 (Gilani & Ahmed, 2015).

$$X_c = 8.09 \times 10^{-4} T(^{\circ}\text{C}) + 0.61341 \quad (3.1)$$

Typically, As the wet solid hydrate is formed, it clings to piping components and discontinue the flow which can result in the imminent shutdown of the process. Furthermore, the crystallization events require considerable time and effect to solve due to the viscosity of the solid hydrate. The common procedure to solve the problem is increasing the temperature of the pipe system and then diluting it with water which can take many hours of plant operating time.

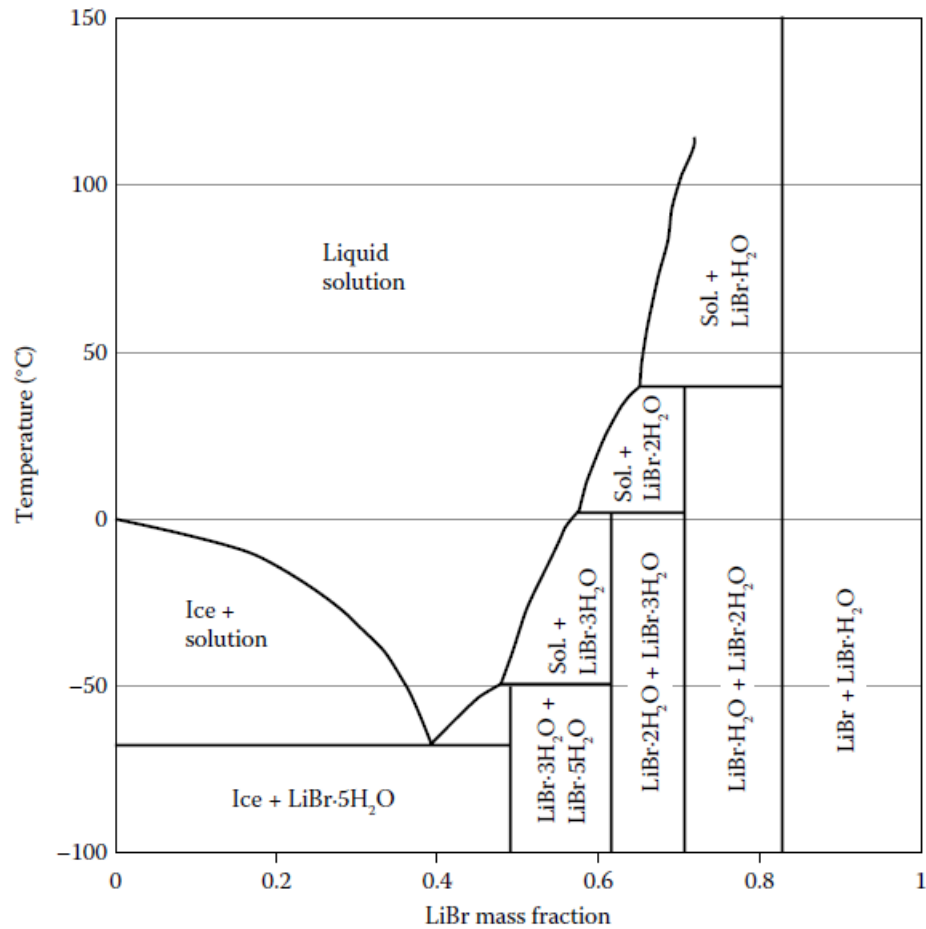


Figure 3.3 Water/lithium bromide phase diagram (Herold *et al.*, 2016)

The relationship of water/lithium bromide solution states at saturated condition also can be determined using Dühring's rule. The rule states that a relationship exists between the temperatures at which two solutions exert the same vapor pressure. So, the saturated temperature of the solution can be calculated as a function of a mass fraction of the components and the saturated temperature of any pure component such as water. All Thermophysical properties of aqueous lithium bromide solution used for calculation are obtained from 2009 ASHRAE handbook and the details of the properties are shown as follows

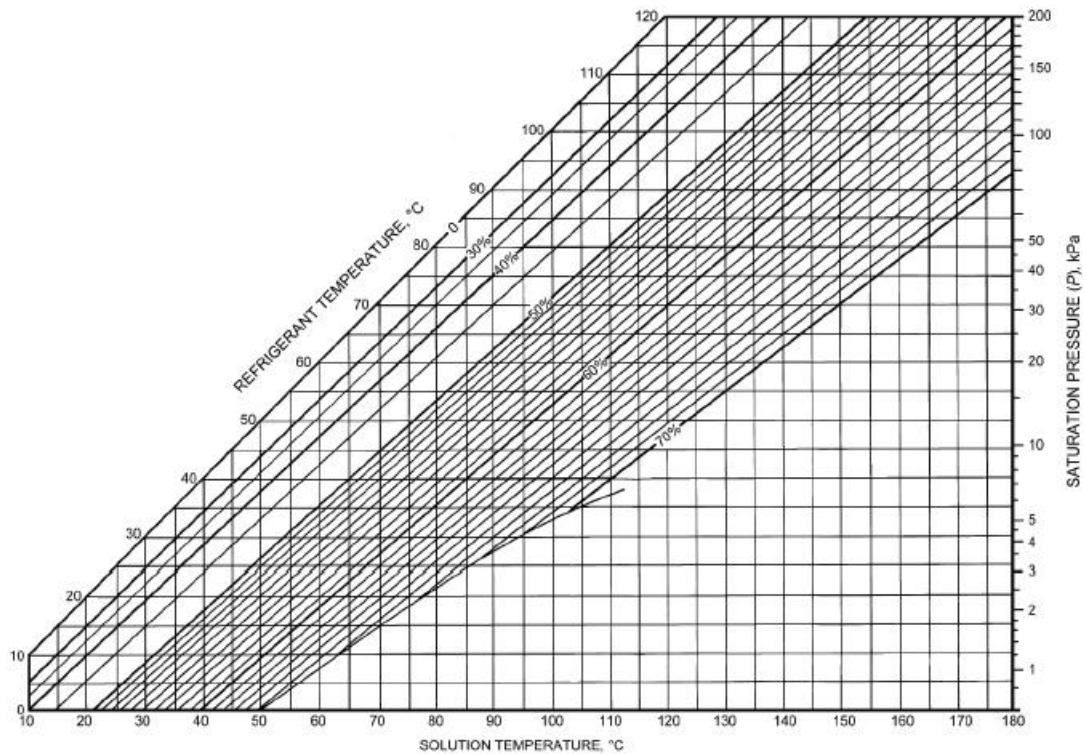


Figure 3.4 Water/lithium bromide Dühring's chart (*ASHRAE handbook: Fundamentals, 2009*)

Equation

$$t = \sum_0^3 B_n X^n + t' \sum_0^3 A_n X^n, \quad t = \text{Solution Temperature } ^\circ\text{C}, \quad t' = \text{Refrigerant Temperature } ^\circ\text{C}$$

$$T' = \frac{-2E}{D + [D^2 - 4E(C - \log P)]^{0.5}}, \quad T' = \text{Refrigerant Temperature K}, \quad P = \text{Pressure kPa}$$

$$A_0 = -2.00755$$

$$B_0 = 124.937$$

$$C = 7.05$$

$$A_1 = 0.16976$$

$$B_1 = -7.71649$$

$$D = -1596.49$$

$$A_2 = 3.133362E - 3$$

$$B_2 = 0.152286$$

$$E = -104095.5$$

$$A_3 = 1.97668E - 5$$

$$B_3 = -7.95090E - 4$$

Range $-15 < t' < 110^\circ\text{C}$

$$5 < t < 175^\circ\text{C}$$

$$45 < X < 70^\circ\text{C}$$

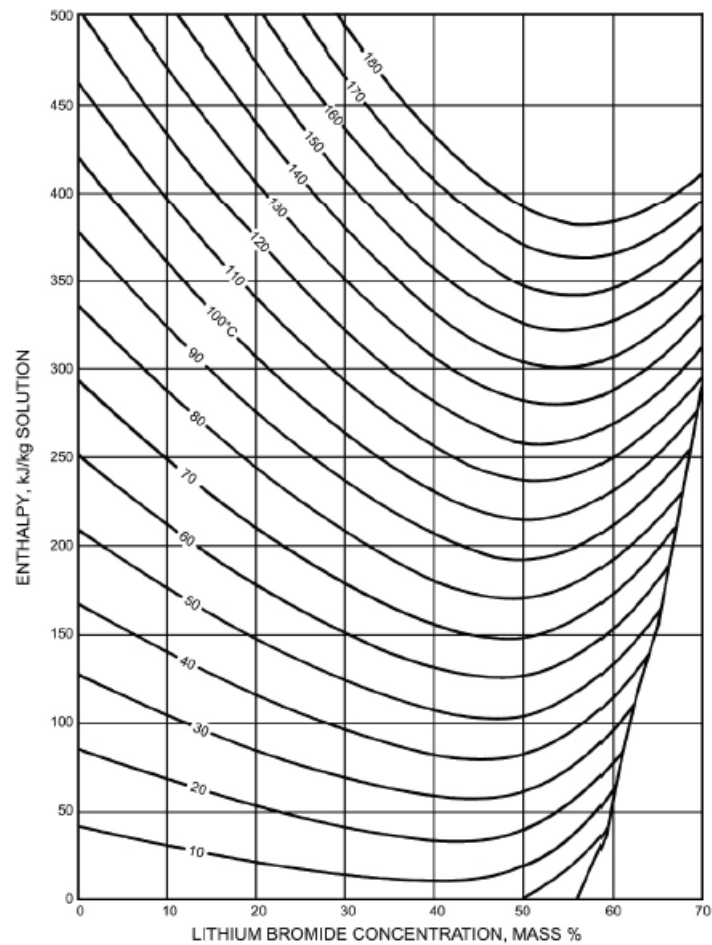


Figure 3.5 Enthalpy-mass fraction diagram (*ASHRAE handbook: Fundamentals*, 2009)

Equation

$$h = \sum_0^4 A_n X^n + t \sum_0^4 B_n X^n + t^2 \sum_0^4 C_n X^n \quad \text{in kJ/kg}$$

$$A_0 = -2024.33$$

$$B_0 = 18.2829$$

$$C_0 = -3.7008214E - 2$$

$$A_1 = 163.309$$

$$B_1 = -1.1691757$$

$$C_1 = 2.6677666E - 3$$

$$A_2 = -4.88161$$

$$B_2 = 3.248041E - 2$$

$$C_2 = -8.1313015E - 5$$

$$A_3 = 6.302948E - 2$$

$$B_3 = -4.034184E - 4$$

$$C_3 = 9.9116628E - 7$$

$$A_4 = 6.302948E - 2$$

$$B_4 = 1.8520569E - 6$$

$$C_4 = -4.4441207E - 9$$

Concentration Range $40 < X < 70\%$ LiBr Temperature range $15 < t < 165^\circ\text{C}$

3.1.2. Single Effect Water/lithium bromide Absorption Chillers

Single effect water/lithium bromide chiller is one of the simplest heat pump technologies. The absorption cycle is composed of a condenser, an evaporator, an absorber, a solution heat exchanger, and a generator. The cycle starts when the weak aqueous lithium bromide is pumped from an absorber, through a solution heat exchanger, to a generator. In the generator, external heat is supplied, and water is boiled off. After the partial evaporation, steam is sent to a condenser and the concentrated solution is flown back, through a solution heat exchanger and solution expansion valve, to the absorber. In condenser, steam is liquefied existed using cooling utility. Then the liquid water is throttled via a refrigerant expansion valve and sent to an evaporator. At under atmosphere pressure, in the evaporator, the water acts as refrigerant as it consumes heat to complete the evaporation process. In the end of the cycle the vapor flows back to the absorber and absorbed by concentrated solution. Typically, this process also uses the same cooling utility as a condenser.

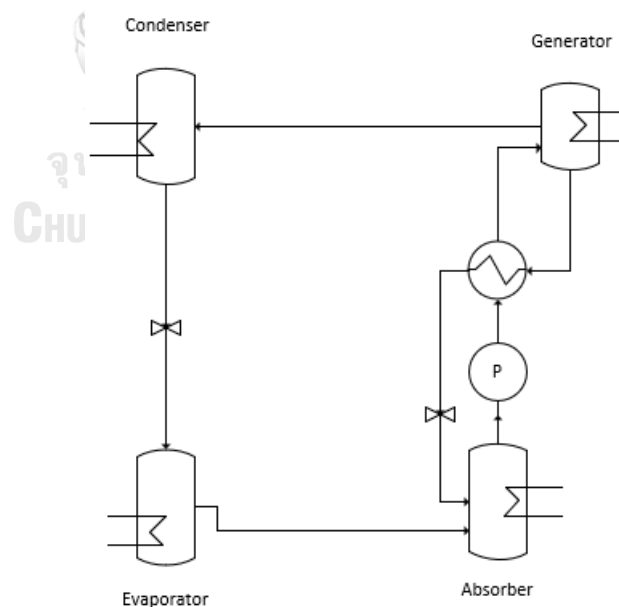


Figure 3.6 A single effect chiller (Herold *et al.*, 2016)

3.1.3. Double Effect Water/lithium bromide Absorption Chillers

The main drawback of single effect absorption chillers is they cannot use the high-quality energy effectively. As, it is reflected in their coefficient of performance (COP) which remains around 0.7 regardless of heat input temperature.

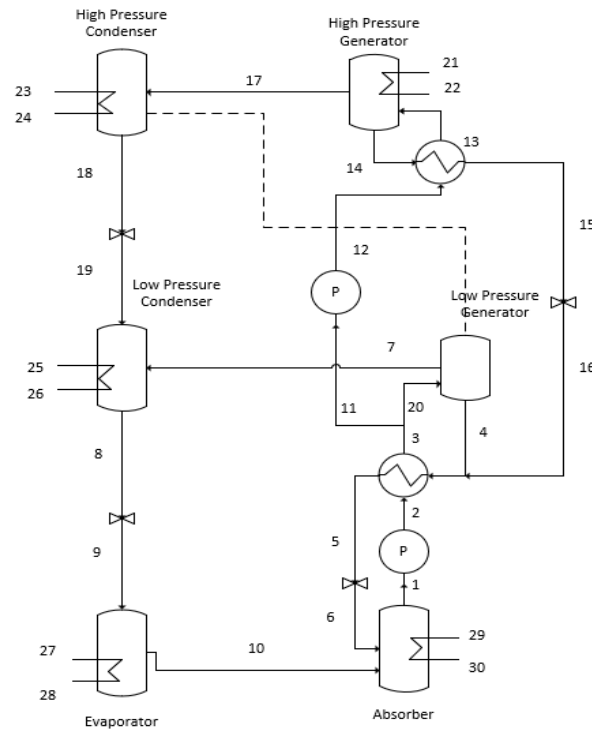


Figure 3.7 A parallel flow double effect chiller (Herold *et al.*, 2016)

Double effect absorption chillers generally double the COP value to around 1 to 1.6. In double effect chillers, there are pairs of solution heat exchangers, condensers and generators. It can provide higher COP due to the heat exchange between a high-pressure condenser and a low-pressure generator, as it provides heat for the low-pressure cycle. For process operating condition, whereas, a low-pressure condenser and generator are operated at almost the same conditions as their counterparts in single effect chillers, the high-pressure condenser and generator require higher temperature and pressure. There are two structure types of double effect absorption chillers; parallel flow and series flow arrangements. The difference is, in in parallel flow, LiBr solution is splitted in to two portions; one entering a low-pressure cycle, and another enter a high-pressure cycle. On the other hand, in series flow, LiBr solution enters both low and high-pressure cycle sequentially. In general,

parallel flow chillers provide higher COP but require more effort to handle as maintaining the correct flow split can be challenge.

Figure 3.8 shows a parallel flow double effect chiller cycle and the approximated position of each stream in the Dühring chart. As illustrated in the chart, the streams leaving a low-pressure generator to an absorber, especially stream 6, are operated near the crystallization line and need to be monitored closely.

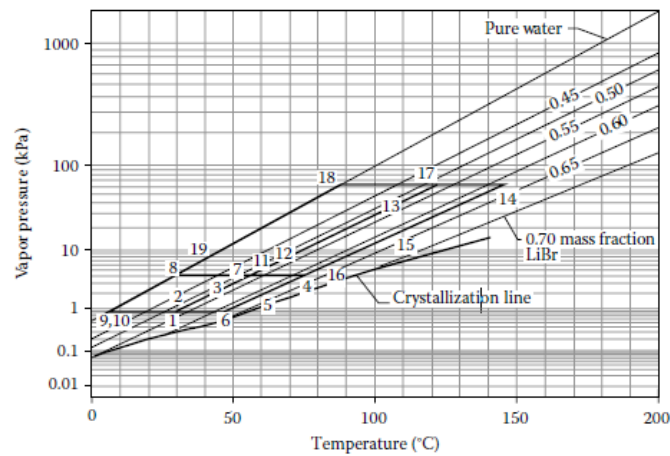


Figure 3.8 Dühring state plot for a parallel flow chiller (Herold *et al.*, 2016)

3.1.4. Heat Exchanger

In typical absorption chiller model, two types of heat exchanger model are used. A heat transfer effectiveness model is used for both of solution heat exchangers and a heat transfer coefficient model is used for the heat transfer between a high-pressure condenser and a low-pressure generator.

In heat transfer effectiveness model, the performance of the heat exchanger is defined as a ratio between actual heat transfer and its maximum possible value and assumed to be constant.

$$\epsilon = \frac{Q_{act}}{Q_{max}} \quad (3.2)$$

Where Q_{max} is defined as a multiplied result between mass minimum heat capacity rate (mC_p) and the maximum temperature difference in the system. For

instance, in case of a counter current flow heat exchanger which the minimum heat capacity rate is at cool steam, the heat transfer effectiveness is defined as

$$\epsilon = \frac{m_c C_{p,c}(T_{c,out}-T_{c,in})}{m_c C_{p,c}(T_{h,in}-T_{c,in})} = \frac{(T_{c,out}-T_{c,in})}{(T_{h,in}-T_{c,in})} \quad (3.3)$$

On the other hand, for heat transfer coefficient model, the heat transfer is determined as Eq. 3.4 as $T_{LMTD} = \frac{(\Delta T_1 - \Delta T_2)}{\ln(\Delta T_1) - \ln(\Delta T_2)}$ and the coefficient (U) is the function of various variables such as flow rates, temperature and pressures. In this study it is also assumed to be constant.

$$Q = UA\Delta T_{LMTD} \quad (3.4)$$

3.2 Plantwide Control Strategy

Plantwide control strategies are methods to design control structures for an entire plant with emphasizing on the structural decisions. In practice, the control system of a chemical plant is usually divided by a time-scale or “horizontal decomposition” into five control layers as shown in Figure 3.9. The first three layers on the top; scheduling, site-wide optimization and local optimization are deal with economic and logistic aspect of plant and typically be done manually. So, the main focus for the control structure design is in the last bottom two layers. The regulatory layer mainly deals with plant stability such as inventory and pressure control, and the supervisory layer duty is dealing with optimization of the process to achieve plant objectives.

The structural decisions for those layers are expressed below,

- Decision 1: Select primary controlled variables (CV1) for the supervisory control layer. The setpoints is link the process optimization with supervisory control layer.
- Decision 2: Select secondary controlled variables (CV2) for the regulatory control layer. The setpoints link the supervisory and regulatory control layers.

Decision 3: Locate the throughput manipulator (TPM) location. it links the top-down and the bottom-up parts of the economic plantwide control.

Decision 4: Select pairings for the stabilizing layer controlled variables.

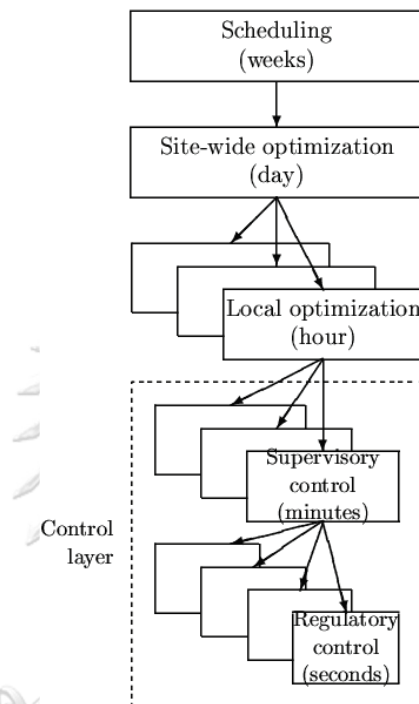


Figure 3.9 Plant horizontal decomposition diagram (Skogestad, 2004)

In order to make those four decisions, Skogestad's procedure (2004), consists of seven steps as follows

Top-down analysis part

Step 1: Define the operational objectives

Step 2: Optimize process nominal operating conditions

Step 3: Select primary (economic) controlled variables

Step 4: Select the location of throughput manipulator (TPM)

Bottom-up control structure design part

Step 5: Design the control structure of the regulatory control layer

Step 6: Design the control structure of the supervisory control layer

Step 7: Design the control structure of the local optimization layer (optional, not include in this work)

3.2.1. Define the Operational Objectives

The first step is assessing the objective of the plant which determine the setpoints of primary controlled variables which is an important step because it can be influenced on all of the following steps and the control structures. Normally, the objective of the process is minimizing the singular economic cost function (J). Operation constraints such as safety conditions, upper and lower limits of manipulated variables, pressure, temperature, product specifications and limitation of equipment are also addressed in this step.

3.2.2. Selection of Manipulated Variables, Degree of Freedom Analysis and Steady State Optimization

After the objective function is defined, a starting point for design the plantwide control structure is to determine and classify degree of freedom. First, the control degree of freedom (CDOF) and the steady-state degree of freedom are determined. The control degree of freedom is the number of variables that can be control independently including flowrate, temperature, pressure and concentration. The number also equals to the number of manipulated variables of the process or “physical degree of freedom”. Theoretically, the CDOF can be determined by the number of variables subtracted by the number of independent equations. However, this method is error-prone as it is easy to miss either some equations or variables (Larsson & Skogestad, 2000). The more practical way is to count the number of adjustable valves across the process then add by the number of adjustable electrical or mechanical variables

The steady-state degree of freedom is the number of independent variables that can be used for steady-state optimization. It can be determined by subtracted CDOF by the number of manipulated inputs with no steady state effect (N_{m0}) as well as the number of manipulated inputs used to control variables with no steady-state effect (N_{y0}). Whereas the former is uncommon in typical chemical processes, the

most prominent case of the latter is manipulated variables used to control liquid level in buffer tanks.

$$N_{ss} = CDOF - N_{m0} - N_{y0} \quad (3.5)$$

It is also beneficial to reduce the complexity of the optimization problem using some process insight to pre-determine which constraints should be active at the optimal condition. Number of “free” steady-state degree of freedom is determined by the steady-state degree of freedom minus number of active constraints. Then the steady-state optimization problem can be formulated as

$$\begin{aligned} & \min_u J(u, x) \\ \text{s. t.} & \quad g_1(x, u) = 0 \\ & \quad g_2(x, u) \leq 0 \end{aligned}$$

Moreover, the major disturbances and their range are identified in this stage. The most common disturbances are including with the feed rate and the composition, the external temperature and the pressure as well as the change in product specifications, the capacity constraints and process parameters such as rate constants and efficiencies.

3.2.3. Select Primary (economic) Controlled Variables

Selection of the control variables to achieve self-optimizing control is the featured concept of Skogastad’s plantwide control procedure. Its main idea is presented in Figure 3.10. In the figure, z_1 and z_2 are control variable candidates (z) which setpoint optimized at the nominal operating conditions with disturbances equal to \bar{d} , so that the loss, defined as the difference between the actual cost function and the optimal one at the same disturbance, is equal to zero. As the disturbance changes, the process is shifted from the nominal point and those setpoints are not optimal anymore. One way to reduce the loss is to add an online optimizer to keep the process at optimal condition at all time. However, it adds more complexity as well as model dependence to the control structure.

Differently, concept of self-optimizing control is to find the control variables which make the plant achieves desired performance regardless of disturbances, while

they held constant. For instance, as illustrated in Figure 3.10, difference control variables lead to difference loss and in this case z_1 is a better self-optimizing control variable.

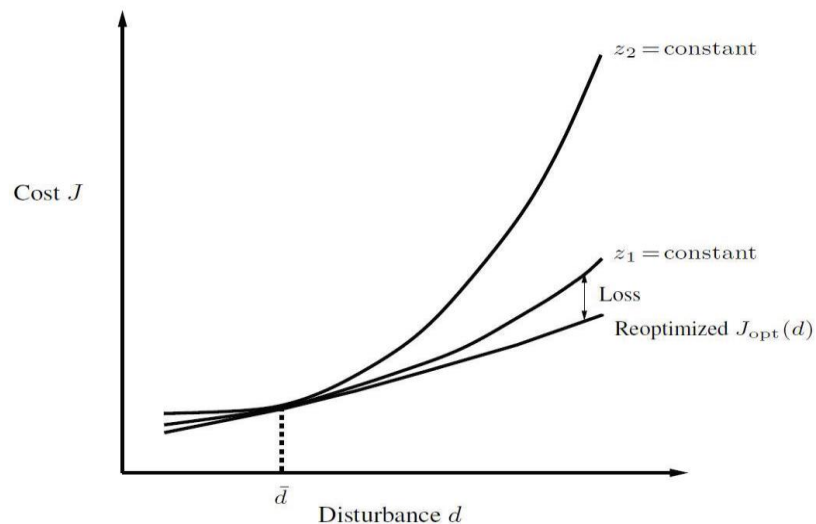


Figure 3.10 Loss incurred by keeping constant setpoint for different control variables (Skogestad, 2000)

The first step to identify the self-optimizing control variables is using the qualitative rules to determine a set of candidates. Characteristic of the promising candidates for are listed as follows (Skogestad, 2000)

1. Optimal value of control variables should be insensitive to disturbances to minimize setpoint error.
2. The control variables should be easy to measure and control to ensure small implementation error.
3. The control variables should be sensitive to the change in manipulated variables to minimize the deviation of manipulated variables from the optimal value.
4. For cases with more than one control variables, the variables should not be closely correlated.

As the set of candidates are acquired, there are many ways to find the variables. The most direct way is to formulate the mixed integer nonlinear programming (MINLP) optimization problem and solve it by various techniques or brute force. However, due to complexity of the optimization, this method may be not feasible for complicated systems.

Another approach is a local method as it changes the problem to a less complex one that can be solved by utilizes existed linear analysis tools. The methods used in this study is minimum singular value (MSV) and null space method. For MSV, a second-order Taylor series expansion is applied to the cost function at operating point and the loss (L) can be calculated as follow (Halvorsen *et al.*, 2003)

$$L = \frac{1}{2}(u - u_{opt})^T (J_{uu})(u - u_{opt}) \quad (3.6)$$

Then, for any certain disturbance, Δz can be estimated as $G\Delta u$ where G is a steady-state gain matrix from u to z

$$L = \frac{1}{2}(z - z_{opt})^T G^{-T} (J_{uu}) G^{-1} (z - z_{opt}) \quad (3.7)$$

So, the worst-case loss in singular form can be derived as

$$L_{worst-case} = \frac{|J_{uu}|}{2|S_i G|^2} \quad (3.8)$$

Where a scale matrix $S_i = \frac{1}{\min_d |z_i - z_{i,opt}|}$. And since the value of $|J_{uu}|$ is independent from the choice of z , the most suitable control variables can be determined as the candidates that provide the highest $|S_i G|$.

As for null space method, rather than using one measurement (z) for each control variable (C), proper linear combinations of the measurement by matrix H as shown in Eq 3.9 can, theoretically, further improve the structure effectiveness.

$$C = Hz \quad (3.9)$$

Null space ($N(A)$), also known as kernel, is a concept in linear algebra. Basically, they are a set of vectors that lose all their information and impact as they operate with a system matrix (A) and vice versa.

$$N(A) = \{x \in R^n \mid Ax = 0\} \quad (3.10)$$

Consequently, from Eq. 3.9 at optimal point; $\frac{\partial C_{op}}{\partial d} = H \frac{\partial z_{op}}{\partial d}$ with an assumption that all components in the matrix $\frac{\partial z_{op}}{\partial d}$ are constant, $\frac{\partial C_{op}}{\partial d}$ will equal to zero as

$$H = N\left(\frac{\partial z_{op}}{\partial d}\right) \quad (3.11)$$

It means that the optimal value of the combined control variables will be the same regardless of disturbance. However, as in real process $\frac{\partial z_{op}}{\partial d}$ is not a linear time-invariance matrix, the loss from the combined variables will not be completely nullified. Nevertheless, it should provide better results compared to individual variables. The main limitation of the method is in order to calculate matrix H , number of combined measurements (z) has to be higher or equal to number of disturbance (d) plus manipulated variables (u).

3.2.4. Set the Throughput Manipulator (TPM) Location

The location of throughput manipulator (TPM) is depended on the plant mode of operation which includes on-supply, on-demand and on-internal. The mode of operation is ultimately depended on the propose of the plant such as on-demand production (Buyer market) or maximize productivity (Seller market). For maximize productivity, TPM should be set at the bottom neck of the process which usually is inside the process (on-internal mode of operation). On the other hand, for the on-demand and on- supply production plant, the location of throughput manipulator has been set at product stream and feed stream respectively.

3.2.5. Bottom Up Control Structure Design

In this step, two type of controller are applied; model predictive controllers (MPC) for multiple-input and multi-output (MIMO) system and PID controllers for decentralized single-input and single-output (SISO) systems.

As a typical process nowadays behaves as one large complex MIMO system, the optimal way to control it mathematically is using one large multivariable

centralized controller. One of the most prominent controllers in the case is MPC. The controller was developed in the 1970s by two research groups. Dynamic Matrix Control (DMC), devised by Shell Oil (Cutler and Ramaker, 1980) and ADERSA (Richalet *et al.*, 1978). Its main feature is ability to handle changing in disturbance and constraints with high performance. However, it requires accurate multivariable dynamic model and its complexity lead to problems in troubleshooting.

The main concept of model predictive control is using plant model to calculate the proper changes in manipulated variables, leading control variables to desired stages based on current and predictions of the future values of the state variables. The objective of the MPC control is to determine a sequence of inputs for certain period, i.e. control horizon, so that after certain interval, i.e. prediction horizon, the states are as close to the setpoints as possible. Normally control horizon is much smaller than prediction horizon and past the control horizon, the input is held constant for the rest of the prediction horizon. The main difference between MPC and other optimal controls is that, even though a sequence of inputs is calculated for entire control horizon, the controller only implements the first set of the manipulated variables to the actual process and then repeat the calculation for the next interval.

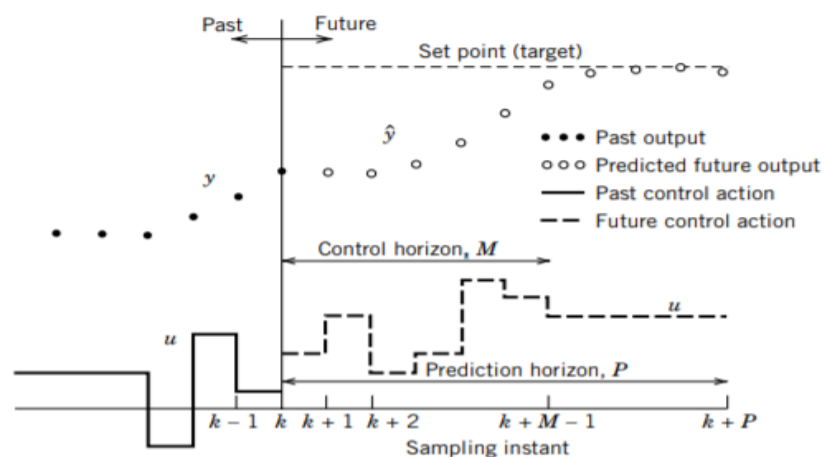


Figure 3.11 MPC concept (Seborg *et al.*, 2010)

The typical objective function of MPC is shown as Eq 3.12 where W_1 is weight on the control variables, W_2 is weight on the manipulated variables and t_f is the prediction horizon. The flexibility of the objective function is another feature point

of the controller as it can be customized freely, and constraints can be added when necessary.

$$\min \int_0^{t_f} \{W_1(X - X_{sp})^2 + W_2(\Delta U)^2\} dt \quad (3.12)$$

The downside of a MIMO centralized controller is such controller obligates high demands on control configuration as well as computer processing. Its performance also depends on model accuracy. Furthermore, most plants and technology providers in chemical industry still used to basic SISO control systems and do not have neither motivation nor capability to adapt to the new system.

On the other hand, an alternative is a decentralized control. It is a simpler approach as it divides the plant control structure into multiple non-interacting feedback SISO control loops. While decentralize control may never outperform a perfect tuned multivariable centralized controller, it has many advantages including

- i. Inherent simplicity to design and operate
- ii. Local units can act quickly to reject disturbance
- iii. Flexibility to adjust and tuning the process and change control objective
- iv. More failure tolerance as it is able to maintain some degree of control while a subsystem is failing
- v. Less sensitive to model uncertainty

The task of designing a decentralized control system can be split into two separate sub-problems:

- i. Determine subsets of input-output pairs in such a way that the control-loop interactions be minimized.
- ii. Design a controller for each input-output pair.

For the first task, there are three groups of input-output selection methods, relative gain array methods (RGA), interaction measures (Grosdidier *et al.*, 1985) and methods based on controllability and observability analysis.

The method used in this work is steady-state RGA (Bristol, 1966) . In this method, the corresponding relative gain λ_{ij} is defined as the ratio between the open-

loop gain ($g_{ij}(0)$) and the loop gain where all the outputs except the interested one are under tight control ($[G^{-1}(0)]_{ji}$) as shown in Eq. 3.13. Moreover, the dynamic relative gain array (DRGA), the RGA for any given frequency can be determined by substituting $G(0)$ with $G(\omega i)$ Eq. 3.14 (McAvoy, 1983). The details for the value of λ_{ij} are summarized in Table 3.2.

$$\lambda_{ij} = \frac{g_{ij}(0)}{[G^{-1}(0)]_{ji}} \quad (3.13)$$

$$\lambda_{jk} = \frac{g_{ij}(\omega i)}{[G^{-1}(\omega i)]_{kj}} \quad (3.14)$$

Table 3.2 Meaning of the value of λ_{ij} (Skogestad & Postlethwaite, 1996)

Values of λ_{ij}	Meaning
< 0	Conflicting gain as open loop and closed-loop gains have different sign. Other loops will affect the pairing in undesirable ways, thus, this input-output pair should be avoided
0	The input does not have any effect on the output, thus, this input-output pair should be avoided
0-0.5	The pair have some degree of interaction
0.5-1	Whereas there is influence from other loop, the interaction of this input-output pair is dominance, thus, this is a preferred pair.
1	The interaction between open loop and closed-loop gains is identical and this is a preferred pair.
>1	The interaction from other loops will reduce the gain of this input-output pair. As the number increases, the effect is more severe.

For the controller, a proportional–integral–derivative controller (PID) and its various, especially PI controller, are the most widespread controllers in the industry. The controller model is shown as Figure 3.12. In most tuning methods the information required to properly tune a PID controller is a transfer function between an input and output. The function can be acquired either directly from process model or via system identification. The most common transfer function used in chemical industries is a

first order with a time delay model as shown in Eq 3.15 as it can represent most of process dynamic and provides enough information from PI controller tuning.

$$y = \frac{k}{\tau s + 1} \exp(-\theta s) u \quad (3.15)$$

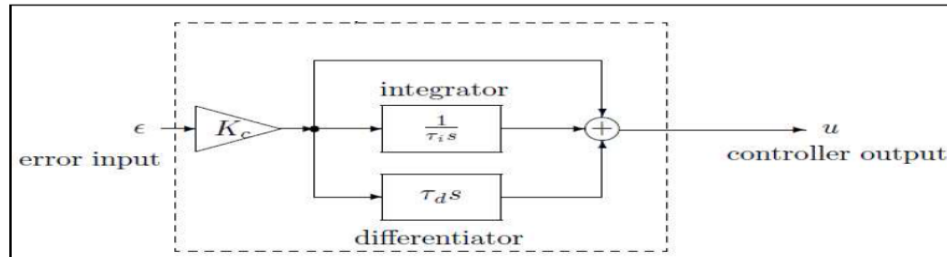


Figure 3.12 PID model



CHAPTER IV

ABSORPTION CHILLER PROCESS CHARACTERISTIC AND DESIGN

This chapter presents the procedure for developing the mathematical models of the adsorption chiller process and the validation.

4.1 Absorption Chiller Models

In order to create the mathematical models of the adsorption chiller for studying the dynamic behavior of the process, the mass and energy balance technique was applied to each unit inside the process. Figure 4.1 demonstrates all units inside the adsorption chiller process. Moreover, the following assumptions were formulated for developing the models in this work.

1. Only water was vaporized in generator, so the refrigerant was pure water.
2. The refrigerant left condensers and evaporator at saturated states.
3. The water-LiBr solution leaving the absorber and generators was saturated.
4. The refrigerant leaving the generators was at saturated temperature of the water-LiBr solution entering the generator.
5. The temperature of the solution leaving the absorber was equal to the temperature of the refrigerant leaving the low-pressure condenser.
6. The system was operated at three pressure levels depended on temperature of desired chilled water, temperature of cooling utility and temperature of the heat input.
7. Valves were isenthalpic devices.
8. Work of pumps, heat losses to the environment, pressure drop and fluid transport delays between components were neglected.
9. Level in each unit had linear relation with its liquid holdup. And all level in this work was represented by the holdup.

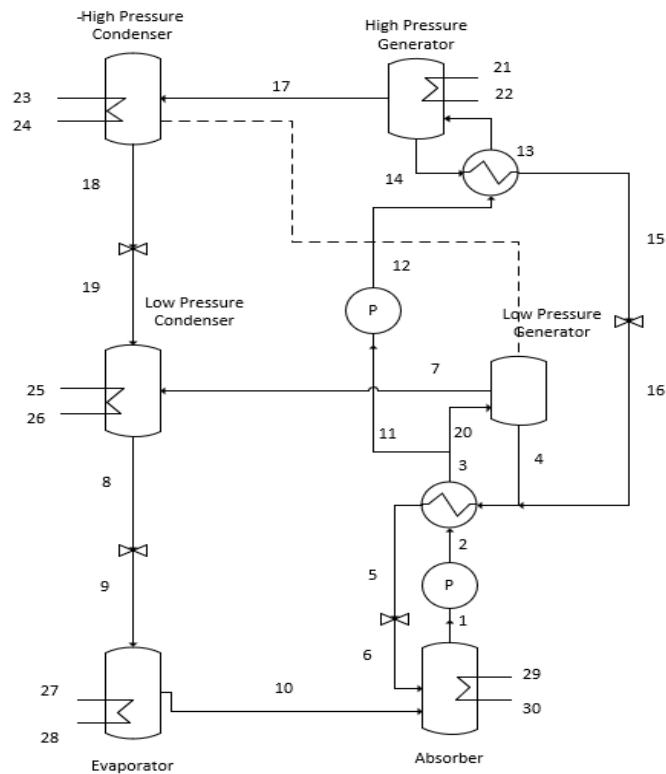


Figure 4.1 A parallel flow double effect chiller

For each unit mass, energy and component balance of the LiBr solution are shown as follows

$$\frac{dM}{dt} = \sum m_{in} - \sum m_{out} \quad (4.1)$$

$$\frac{dH}{dt} = \sum m_{in}h_{in} - \sum m_{out}h_{out} + Q \quad (4.2)$$

$$\frac{dMX}{dt} = \sum m_{in}x_{in} - \sum m_{out}X \quad (4.3)$$

For liquid mass flowrate leaving each unit, a control valve coefficient (C_m) was defined so that

$$m_{out} \approx kC_v\sqrt{M}, \quad k = \text{constant} \quad C_v = \text{flow coefficient} \quad (4.4)$$

For the solution heat exchanger, the heat transfer effectiveness was applied as

$$\epsilon = \frac{Q_{act}}{Q_{max}} \quad (4.5)$$

Heat transfer between a high-pressure condenser and a low-pressure generator, the heat transfer coefficient was applied as

$$Q = UA\Delta T_{LMTD} \quad (4.6)$$

And the splitting ratio was defined as

$$R = \frac{m_{20}}{m_3} \quad (4.7)$$

4.2 Mathematical Model Validation

To validate the developed mathematical models, simulation results from the developed models were compared with the three sets of data obtained from the cited literatures; energy values at nominal operating conditions, relation between COP and temperature of a high-pressure generator (T_{g2}) with constant pressure, and relation between COP and splitting ratio with constant T_{g2} . The validation results are shown in Table.4.1, Figure 4.3 and Figure 4.4.

Firstly, all heat flow input and output of the process were compared to data from Herold (2012) with T_{g2} , a low-pressure condenser (T_{c1}) and an evaporator (T_e) as well as splitting ratio (R) equal to 144.68, 29.68, 5.24°C and 0.432 respectively. Table 4.2 shows that the developed models provides a good agreement with error around 1.85% when compared with the reference data. The most difference is amount of cooling utility in a low-pressure condenser with 4.04% error.

Table 4.1 Comparison of major energy transfer between simulation results and data from Herold *et al.* (2016)

	Simulation	Data	Error (%)
COP	1.384	1.359	1.87
Q_a (kW)	443.1	442.5	0.14
Q_e (kW)	367.4	360.6	1.89
Q_{g2} (kW)	265.4	265.4	-
Q_{g1} (kW)	204.5	201.9	1.29
Q_{c1} (kW)	191.0	183.6	4.04

The second part of the validation was comparing effect of temperature in a high-pressure generator on COP. This was the most common way to validate an

absorption chiller results in literatures as it shows an interesting characteristic of the absorption chiller system. As when all pressure levels were held constant, there was a soft limit in COP the chiller can yield regardless of the temperature in a high-pressure generator. The limit could be changed depended on specification of the chiller though. For instance, as show in Figure 4.2 with T_{c1} and splitting ratio equaled to 32°C and 0.5, as T_e dropped from 15°C to 5 °C, the maximum COP was dropped from 1.6 to 1.4. For the validation, simulation result at T_e equals 15°C was compared with data from Khan *et al.* (2017). Figure 4.4 shows that the developed models result agreed well with the reference data with the error around 3.08 %.

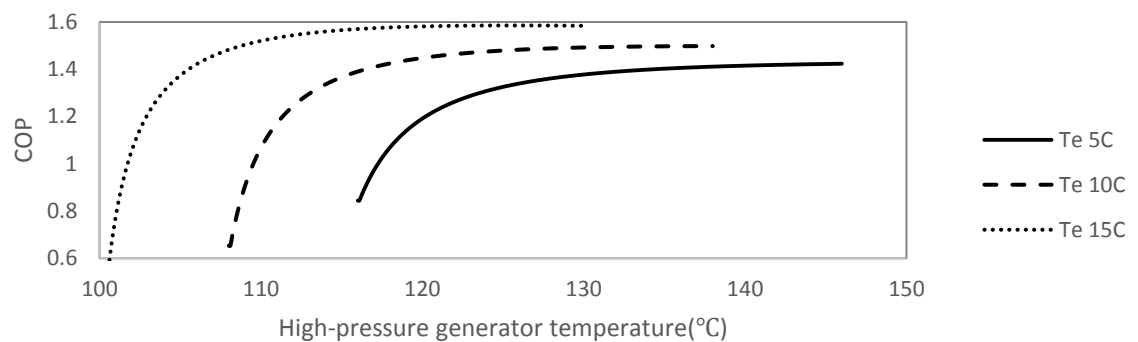


Figure 4.2 COP as a function of temperature in a high-pressure generator

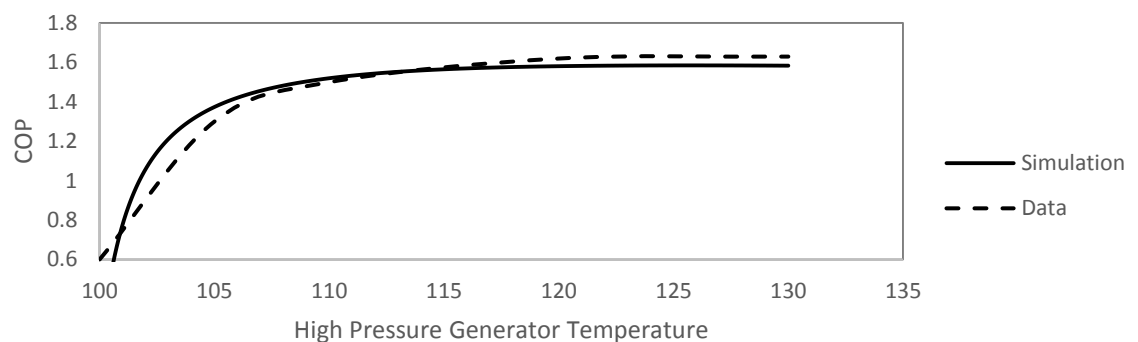


Figure 4.3 Comparison of simulation results and data from Khan *et al.* (2017)

The last scenario was the control scheme used in this work. In this case, rather than constant pressure, temperature in a high-pressure generator was controlled to be constant. The main benefit of this scheme was the difference between heat input and the generator temperature was constant even when the splitting ratio changed to optimize the process. Figure 4.4 shows the compared result between a simulation and

data from Dixit (2016) as T_{g2} , T_{c1} and T_e are equaled to 155, 29.4 and 7.2 °C, the error was around 1.8% however it was schematic as the simulation COP is higher for all the splitting ratio. Consequently, the model was verified, and design specifications used in the case study are shown in Table 4.3.

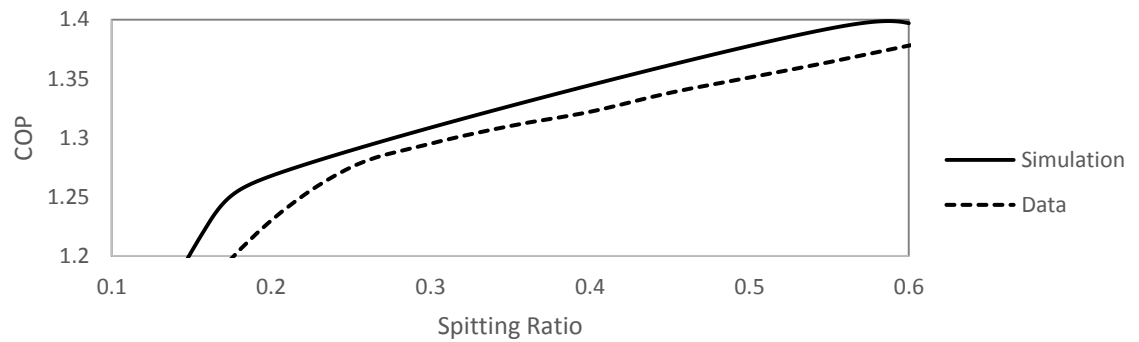


Figure 4.4 Comparison of simulation results and data from Dixit (2016)



Table 4.2 Design specifications

Nomenclatur			
e	Value	Unit	Comments
T_{21}	170	°C	Heat source (0.79 MPa saturated steam) temperature
T_{g2}	$T_{21}-15$	°C	
T_{25}	29	°C	Cooling utility temperature
T_{c1}	$T_{25}+3$	°C	
T_a	$T_{25}+3$	°C	
T_{28}	7	°C	Chilled water temperature
T_e	$T_{28}-2$	°C	
m_1	60	kg/min	LiBr solution flowrate
ϵ	0.64	-	
UA_{g1}	600	kJ/(°C min)	UA for the heat transfer between c_2 and g_1
Mass inventories			
M_a	85	Kg	
M_e	55	Kg	
M_{c1}	30	Kg	
M_{c2}	30	Kg	
M_{g1}	90	Kg	
M_{g2}	150	Kg	
For on-supply mode			
	15,68		
Q_{g2}	0	kJ/min	
For on-demand mode			
	21,12		
Q_e	0	kJ/min	100 USRT / 352 kW

* Most of the specification are loosely based on Herold *et al.* (2016)

CHAPTER V

TOP-DOWN PLANTWIDE CONTROL

In this chapter, top-down analysis of the control structure was performed. This included four steps; define the operational objectives, optimize process nominal operating conditions, select primary (economic) controlled variables and select the location of throughput manipulator.

5.1 Define Operational Objective

Maximizing Coefficient of Performance (COP) was selected as the objective of this work. The coefficient is defined as amount of heat inflow at an evaporator desired temperature, divided by the main required energy input adding to the chiller at a high-pressure generator.

$$\text{COP} = \frac{\text{Useful refrigerating effect}}{\text{Net energy supplied from external sources}} \quad (5.1)$$

In this study either the cooling production rate or energy supplied to the process were set to be constant. So, by selecting maximize COP as the objective function, it also means either minimize heat input for certain production rate or maximize productivity for fix amount of resource. For the constraints, temperature difference between a high-pressure generator, low-pressure condenser and an evaporator, and their utility should be higher or equal to design specification to ensure smooth heat transfer. Also, the flow rate of LiBr solution has to be equal to the design specification. Thereby, the steady state optimization problem should be defined as

$$\begin{aligned} & \max_u \text{COP} \\ \text{s. t.} \quad & T_{g2} \leq T_{21} - 15 \text{ }^\circ\text{C} \\ & T_{c1} \geq T_{25} + 3 \text{ }^\circ\text{C} \\ & T_e \leq T_{21} + 2 \text{ }^\circ\text{C} \\ & m_1 = 60 \text{ kg/min} \end{aligned}$$

5.2 Optimize Process Nominal Operating Conditions

Before the optimization, the degree of freedom analysis was performed. Firstly, control degree of freedom (CDOF) was determined by number of independent manipulated variables in the process. As shown in table.5.1 CDOF of a double effect absorption chiller was eleven.

Table 5.1 CDOF of a double effect absorption

Unit	Amount	CDOF	Type
Absorber	1	1	Heat flowrate (Q_a)
Evaporator	1	1	Heat flowrate (Q_e)
Condenser	2	2	Heat flowrate (Q_{c1}, Q_{c2}) Valve position (Cm_{c1}, Cm_{c2})
High-Pressure Generator	1	2	Heat flowrate (Q_{g2}) Valve position (Cm_{g2})
Low-Pressure Generator	1	1	Valve position (Cm_{g1})
Pump	1	1	Mass flow rate (m_1)
Splitter	1	1	Splitting ratio (R)
Total CDOF		11	

Steady state degree of freedom was calculated by CDOF minus number of manipulated inputs with no steady state effect as well as the number of manipulated inputs used to control variables with no steady-state effect. In this case, the former was equal to zero and the latter was equal to number of controlled liquid inventory control in the process which was five, as solution mass flow rate was controlled instead of liquid level in an absorber. This left six steady states degree or freedom.

For the six steady states degree or freedom, solution mass flow rate of the system was determined by design specification to 60 kg/min, all three temperature constraints in a high-pressure generator, low-pressure condenser and an evaporator should be active, and one was used to set the production rate. That left only one free steady state degree of freedom to optimize the process which is the splitting ratio. So, the steady state optimization problem can be simplified to $max_{ratio} COP$.

In addition, major disturbances were defined as follows; cooling utility temperature varies by $\pm 2^\circ\text{C}$, throughput manipulator varies by $\pm 10\%$, desired chilled water temperature varies by $\pm 2^\circ\text{C}$ and heat input temperature varies by $\pm 5^\circ\text{C}$.

Under the process nominal operating conditions, relations between the splitting ratio and COP for both modes of operation are illustrated in Figure 5.1. From the Figure, the optimal splitting was equal to 0.456 with corresponding COP equal to 1.3467 for both modes of operation. However, for on-demand mode, COP dropped rapidly once pass the optimal point. Moreover, resulted COP when both mode of operation face the disturbance, for instance, when cooling utility temperature changes (T_{c1}) by $\pm 2^\circ\text{C}$, is show in Figure 5.2.

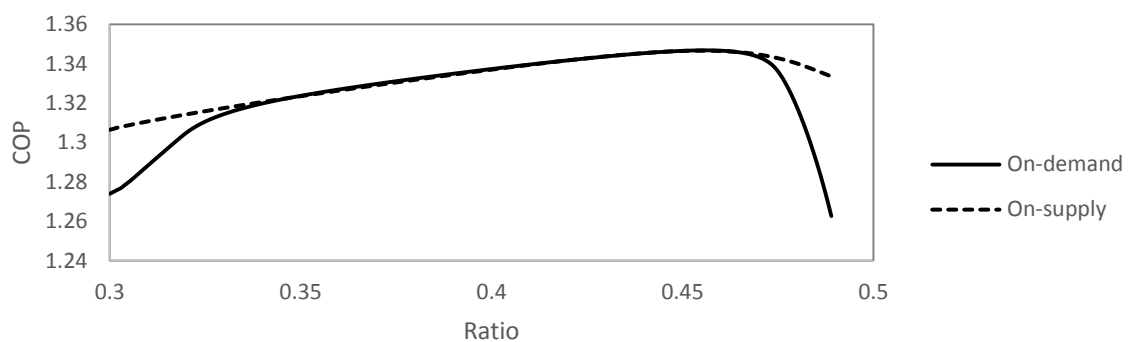


Figure 5.1 COP as a function of splitting ratio at nominal operating condition

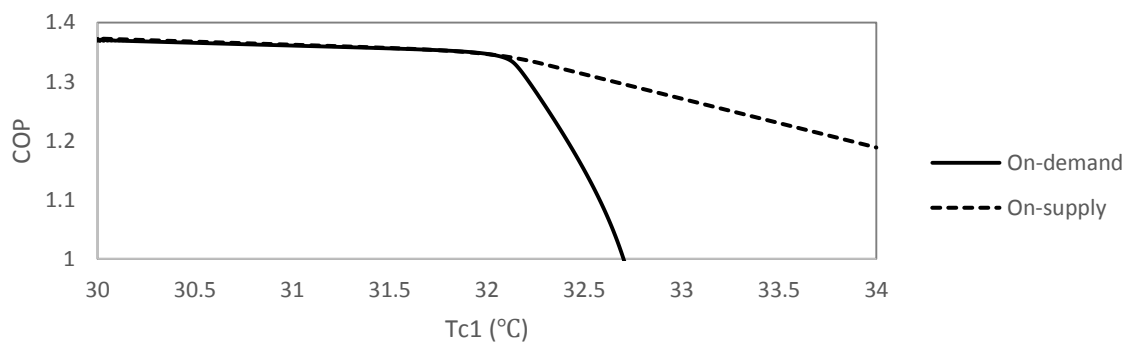


Figure 5.2 COP as a function of a low-pressure condenser temperature

Figure 5.2 shows that, in on-demand mode, the system could not maintain the desired level of COP as the temperature rose. So, to ensure acceptable performance across range of expected disturbance, in this mode, the splitting ratio was set to 0.3 which was the optimal ratio at T_{c1} equal to 34°C instead. This also means that the ratio was not optimal, therefore the self-optimizing control variable was only applied to the on-supply mode of operation.

5.3 Select Primary Controlled Variables

The main task in this step was to find measurements or their combination that behaves as the self-optimizing control variable in supervisory control layer (CV1) for a splitting ratio which was the only free steady state degree of freedom of the process.

5.3.1 Minimum Singular Value

First, according to Skogastad's rule for quantitative approach selection, variables that easy to measure and control were selected as control variable candidates (z). That included mass flowrate, pressure and temperature that had not already held at constraint in previous step. Also, variables that had direct interaction with each other, for instance temperature of the vapor leaving a high-pressure generator (T_{17}) and pressure in high-pressure cycle (P_2) or mass flowrate of the solution leaving the splitter (m_{20} , m_{11}) and the slitting ratio (R), were selected only once. The splitting ratio itself was also a control variable candidate which convey that no additional control variables were needed.

The steady state gain between change in splitting ratio and the control variable candidates were determined using a steady state simulation of the process. The list of the candidates as well as their gain values (G) are shown in Table 5.2. Then, the change in optimal value of each candidate as well as scale matrix (S) were calculated for each case of disturbance independently.

Table 5.2 Gain value of control variable candidates

Control Variable Candidate	Gain
m_4	61.77
m_7	-1.767
m_{14}	-61.13
m_{17}	1.128
P_2	-0.1703
T_3	-25.03
T_4	-64.45
T_5	-19.38
T_{13}	-46.18
T_{15}	-16.02
R	1

MSV index identification as the cooling utility temperature changed

As cooling utility temperature changes from the operating condition by $\pm 2^\circ\text{C}$, a low-pressure condenser and an absorber temperature (T_{c1}, T_a) varied between 30 and 34°C . The relation between spiting ratio and COP with condenser temperature equaled 30°C , 32°C and 34°C are shown in Figure 5.3.

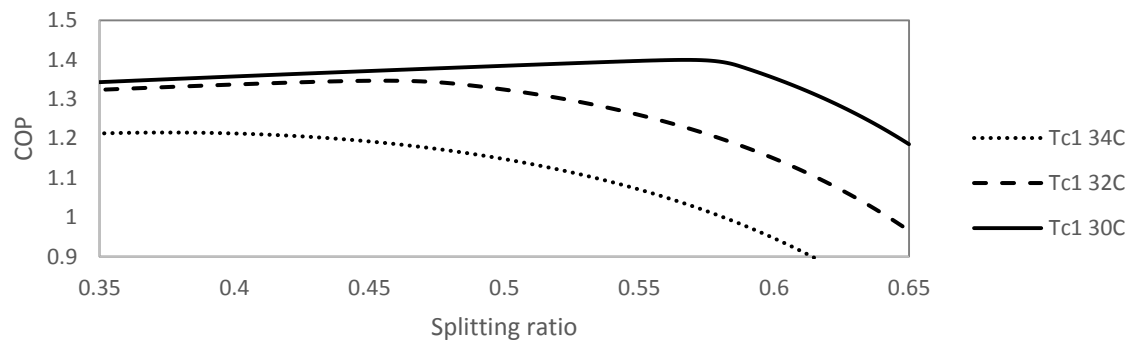


Figure 5.3 COP as a function of splitting ratio as T_{c1} changed by $\pm 2^\circ\text{C}$

As illustrated by the Figure, at nominal condition, the maximum COP was equal to 1.3467 at splitting ratio 0.456 and average COP between ratio 0.35 and 0.65 was 1.2633. As the temperature dropped to 30°C , the average COP was increased to 1.3580 with maximum value equaled to 1.3995 at ratio 0.567. And when the temperature raised to 34°C , the average COP was decreased to 1.0950 with maximum value equals to 1.2151 at ratio 0.375.

The main factor that impact the COP value was the difference in temperature between a high-pressure condenser and a low-pressure generator. As T_{c1} rose, the setpoint of pressure in the condenser also rose in order to maintain saturated state of water output. Since the pressure in the condenser was equal to pressure in generator, the rising in T_{c1} indirectly caused rising in T_{g1} . The narrower temperature gap between high and low-pressure cycle means less energy could be reused in the low-pressure cycle reflected in less overall COP. Moreover, as T_a rose, less vapor could be absorbed. Also, the optimal ratio shifted to lower value indicates that more solution should enter the high-pressure cycle since there was not enough energy input to the lower one. In the same manner, COP was increased, and the optimal ratio shifted higher when T_{c1} decreased.

Table.5.3 shows the change in optimal value for each control variable candidate ($|z_{d,max} - z_{d,min}|$) while the condenser temperature varied from 30°C to 34°C and the index value $\frac{|G|}{|z_{d,max} - z_{d,min}|}$, which was equivalent to $\frac{|S_i G|}{2}$ in the minimum singular value rule. From the Table, the most promising candidate was P_2 as its index value was almost double the others. Other possible candidates were liquid flow rate out of the low and high-pressure generator (m_4 and m_{14}).

Table 5.3 MSV index of control variable candidates as T_{c1} changed by $\pm 2^\circ\text{C}$

z	$ G $	
	$ z_{30^\circ\text{C}} - z_{34^\circ\text{C}} $	$ z_{30^\circ\text{C}} - z_{34^\circ\text{C}} $
m_4	10.59	5.835
m_7	0.9350	1.890
m_{14}	11.74	5.206
m_{17}	0.2213	5.098
P_2	0.01616	10.54
T_3	8.939	2.800
T_4	14.15	4.554
T_5	7.064	2.743
T_{13}	11.10	4.162
T_{15}	5.721	2.800
R	0.1920	5.208

MSV index identification as the amount of heat input to the system changed

In the case that heat input decreased by 10%, the average COP is increased from 1.2633 to 1.3214 with maximum value equals to 1.3635 at ratio 0.567. And when the heat input raised to 10% higher than nominal operating condition, the average COP was decreased to 1.1522 with maximum value equaled to 1.2718 at ratio 0.384.

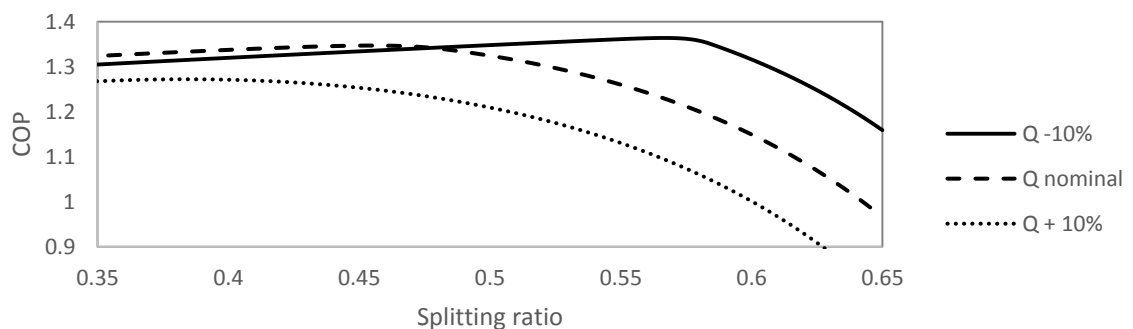


Figure 5.4 COP as a function of splitting ratio as Q_{g2} changed by $\pm 10\%$

As heat input rate increased, amount of heat transfer between the two cycle did not increase in proportionally due to heat transfer limit. Contrarily, the heat transfer was, in fact, decreasing as P_2 was dropped to maintain the generator temperature. So, less portion of heat input could be reuse in lower pressure cycle, resulted in less COP. On the contrary, as heat input decreased, the steam production in a high-pressure generator (m_{17}) also decreased. So, in the region less affected by the heat transfer limit and did not have enough LiBr solution to fully utilize the heat transfer to low pressure cycle, i.e. when the heat input was less than nominal value and the splitting ratio was low, a decrease in heat input resulted in a decrease in COP.

Table 5.4 MSV index of control variable candidates as Q_{g2} changed by $\pm 10\%$

Z	$ z_{+10\%} - z_{-10\%} $	$ G $
		$ z_{+10\%} - z_{-10\%} $
m_4	11.21	5.512
m_7	0.2265	7.801
m_{14}	10.07	6.069
m_{17}	0.9076	1.243
P_2	0.01408	12.10
T_3	2.907	8.612
T_4	10.16	6.343
T_5	3.026	6.404
T_{13}	4.305	10.73
T_{15}	1.860	8.612
R	0.1830	5.464

Table.5.4 shows the change in optimal value for each control variable candidate and its scale gain index value. In this case P_2 was still the best control variable candidate but not by wide margin as the previous case. Furthermore, every candidate except mass m_{17} provided higher scale gain than splitting ratio. The most promising ones other than P_2 were the temperature of LiBr solution that enter a high-pressure generator (T_{13}) and low-pressure generator (T_3) as their scale gains equaled 10.73 and 8.612 respectively.

MSV index identification as the desired temperature of chilled water changed

In the similar way as the changing of cooling utility temperature, changing the desired temperature of chilled water from the operating condition by $\pm 2^\circ\text{C}$, resulted in an evaporator temperature (T_e) varied between 3 and 7°C .

When the evaporator temperature was raised from 5 to 7°C the average COP also increased from 1.2633 to 1.3500 as well as the maximum value which increased to 1.3968 at ratio 0.542. And when evaporator temperature was reduced to 3°C the average COP was decreased to 1.1283 with maximum value equaled to 1.2424 at ratio 0.382.

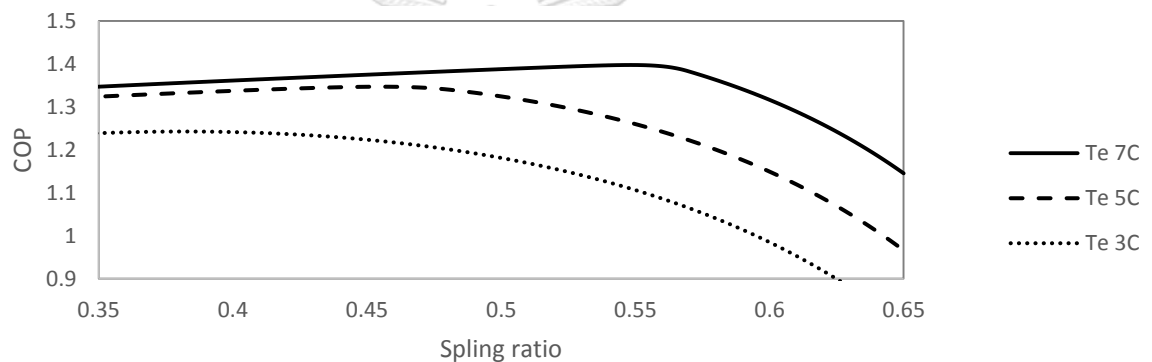


Figure 5.5 COP as a function of splitting ratio as T_e changed by $\pm 2^\circ\text{C}$

The reason was, as T_e increased, pressure in both evaporator and absorber also increased to maintain saturated state of an evaporator outflow. The rise in absorber pressure resulted in more steam absorbed to the LiBr solution, which indirectly increased amount of vapor generation in the generators and COP.

From the scale gain values shown in Table 5.5, P_2 was still, by far, the best candidate as its index was noticeably higher than others.

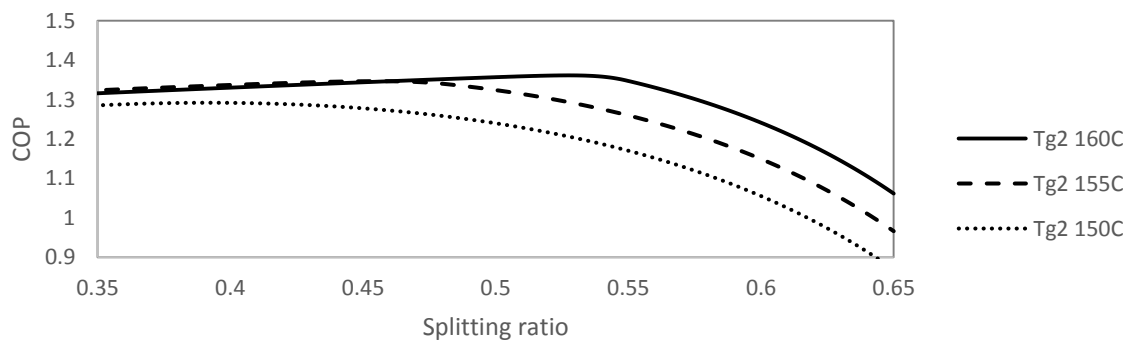
Table 5.5 MSV index of control variable candidates as T_e changed by $\pm 2^\circ\text{C}$

z	$ z_{7^\circ\text{C}} - z_{3^\circ\text{C}} $	$ G $
		$ z_{7^\circ\text{C}} - z_{3^\circ\text{C}} $
m_4	9.205	6.710
m_7	0.7545	2.342
m_{14}	10.20	5.993
m_{17}	0.2403	4.695
P_2	0.009050	18.82
T_3	4.954	5.053
T_4	10.48	6.150
T_5	3.223	6.013
T_{13}	7.964	5.799
T_{15}	3.170	5.053
R	0.1660	6.024

MSV index identification as temperature of heat input changed

Change in temperature of heat input also caused change in temperature of a high-pressure generator. As the input temperature changed by $\pm 5^\circ\text{C}$, the generator temperature (T_{g2}) varied between 150 and 160°C

In the same way as other scenarios, When the generator temperature was raised to 160°C the average COP between splitting ratio 0.35 and 0.65 also increased from 1.2633 to 1.3042 as well as the maximum value which increased to 1.3614 with new optimal ratio at 0.528. And when the generator temperature was decreased to 150°C the average COP was dropped to 1.1883 with maximum value equaled to 1.2919 at ratio 0.392.

**Figure 5.6** COP as a function of splitting ratio as T_{g2} changed by $\pm 5^\circ\text{C}$

In this case as the temperature increased, the generator pressure (P_2) and a high-pressure condenser temperature (T_{c2}) also increased. So, there was more heat transfer between two cycles resulted in higher COP. Contrarily, rise in T_{g2} meant that more heat needed to waste on increasing temperature of the generator inflow (m_{13}) to the generator level. So, as the temperature increased, COP in low splitting ratio region slightly decreased.

Table 5.6 MSV index of control variable candidates as T_{g2} changed by $\pm 5^\circ\text{C}$

z	$ z_{160^\circ\text{C}} - z_{150^\circ\text{C}} $	$ G $
		$ z_{160^\circ\text{C}} - z_{150^\circ\text{C}} $
m_4	7.7802	7.939
m_7	0.3798	4.653
m_{14}	8.239	7.419
m_{17}	0.07909	14.27
P_2	0.001265	134.7
T_3	1.846	13.56
T_4	4.769	13.52
T_5	1.0366	18.69
T_{13}	0.57142	80.82
T_{15}	2.419	6.624
R	0.1360	7.353

From scale gain value shown in Table 5.6, P_2 also had the highest scale gain. However, since the generator temperature is closely correlated to the pressure, reflected in its extraordinary high scale gain, undesired results may be occurred. This is also applied to T_{13} .

Overall MSV index

The overall change in optimal value for each control variable candidate could be calculated by Euclidean norm of the value in each case, defined as Eq.5.2., and the results as well as overall scale gains are shown in Table 5.7.

$$x_{overall} = \|x\|_2 = \sqrt{x_1^2 + x_2^2 + \dots + x_n^2} \quad (5.2)$$

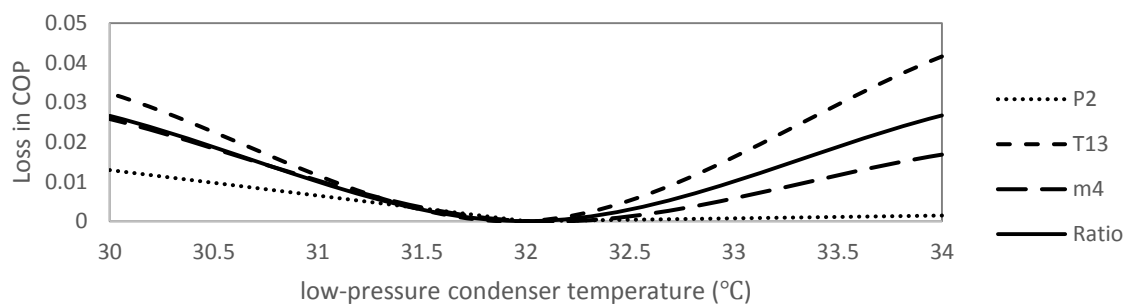
From all previous results, it was a given that P_2 provided the best value and was the best self-optimizing control variable. The second and third promising candidates were T_{13} and m_4 .

Table 5.7 Overall MSV index of control variable candidates

z	$ z_{d,max} - z_{d,min} $	$ G $
		$ z_{d,max} - z_{d,min} $
m_4	19.57	3.157
m_7	1.280	1.380
m_{14}	20.28	3.014
m_{17}	0.9678	1.166
P_2	0.02331	7.310
T_3	10.78	2.321
T_4	20.88	3.009
T_5	8.397	2.308
T_{13}	14.33	3.222
T_{15}	7.217	2.220
R	0.3412	2.931

To verify the effect of the analysis, processes using those three measurements as the self-optimizing control variable were simulated using a steady state simulation.

Figure 5.7 shows the difference in steady state COP between value from self-optimizing control variables and maximum value with optimal splitting ratio at the new state when condenser temperature changes by $\pm 2^\circ\text{C}$. The loss estimation showed a good agreement with the scale gain value from Table 5.3 as P_2 provided the least loss across all temperature compared to other candidates.

**Figure 5.7** COP loss estimation as T_{c1} changed by $\pm 2^\circ\text{C}$

In the case that condenser temperature raised to 34°C , a structure without any self-optimizing variable yielded COP equal to 1.1884 as splitting ratio kept constant at 0.456. On the other hand, while P_2 was held constant, the COP was raised to 1.2137 as the splitting ratio was manipulated from 0.456, to 0.394. Compared to the optimal

COP for this temperature which was 1.2151 at splitting ratio equaled to 0.376, using P_2 as a control variable reduced loss by 94.76%. The similar effect also happened when condenser temperature dropped to 30°C as the splitting ratio was manipulated by P_2 to 0.508 yields COP equaled to 1.3899, whereas the COP at ratio 0.456 was 1.3729 and the optimal COP was 1.3995 at ratio 0.567 resulted in the loss reduction of 51.50%. Another interesting point was when T_{13} was used as a control variable, it yielded more loss than when ratio held constant. This result also matched with the analysis shown in Table 5.3, as in this case, scale gain of T_{13} was less than the scale gain of constant ratio.

Loss estimation in other cases are shown in Figure 5.8 – Figure 5.10 Overall the results agreed with the analysis and confirmed that P_2 was the best control variable. Another interesting result was when temperature in a high-pressure generator was reduced, the loss estimation of T_{13} was less than P_2 even though its scale gain was lower. This happened because P_2 was too sensitive to the change of temperature resulted in too much ratio change. As when the temperature dropped to 150°C, the splitting ratio with P_2 as a control variable was manipulated from 0.456 to 0.363 yielded COP equal to 1.2887, whereas the optimal COP was 1.2919 with ratio at 0.392. The loss reduction in each case as P_2 was used as a control variable is shown in Table 5.8. As shown in the table, the control variable can reduce around 50 – 99 % of loss depend on disturbance.

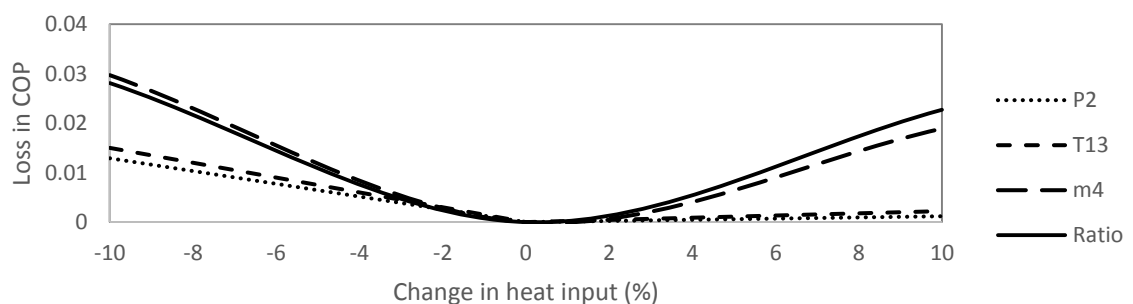


Figure 5.8 COP loss estimation as Q_{g2} changed by $\pm 10\%$

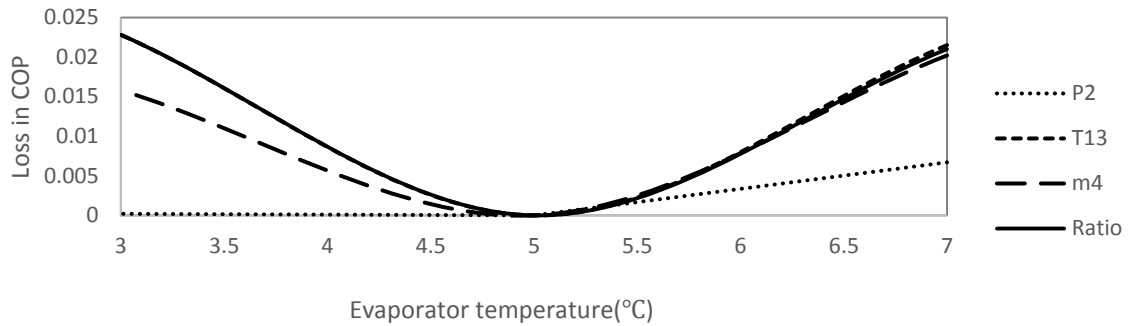


Figure 5.9 COP loss estimation as T_e changed by $\pm 2^\circ\text{C}$

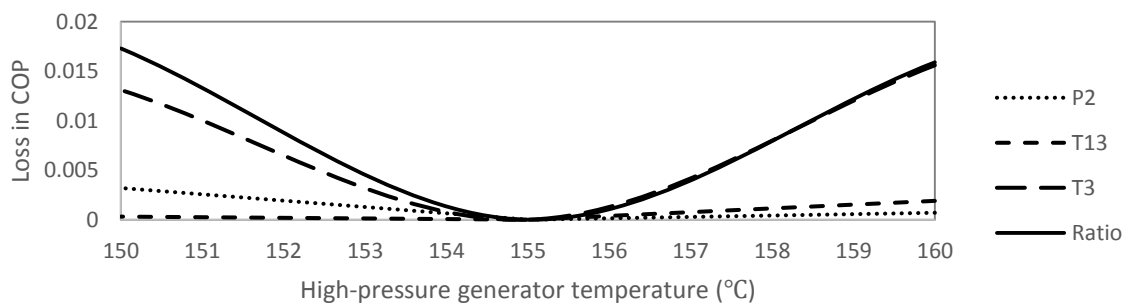


Figure 5.10 COP loss estimation as T_{g2} changed by $\pm 5^\circ\text{C}$

Table 5.8 Loss reduction as P_2 was used as a control variable

$T_{c1}+2^\circ\text{C}$	$T_{c1}-2^\circ\text{C}$	$Q_{g2}-10\%$	$Q_{g2}+10\%$	$T_e-2^\circ\text{C}$	$T_e+2^\circ\text{C}$	$T_{g2}+5^\circ\text{C}$	$T_{g2}-5^\circ\text{C}$
94.76%	51.50%	54.09%	94.71%	99.12%	68.10%	95.60%	81.50%

5.3.2 Null-Space Method

For null-space method, theoretically, as many control variables as possible can be combined to nullify loss from all major disturbances. However due to non-linear nature of the process as well as the fact that balance the combination of many control variables with only a PI controller is a difficult task, combining too many variables may lead to an instability control structure. So, in this work, only three control variables were combined. As for the selected variables, even though T_{13} had slightly higher scale gain, as the temperature outlet from a solution heat exchanger, it was much harder to control compared to m_4 and m_{14} . It was also closely correlated with P_2 . So, the three chosen measurements were P_2 , m_4 and m_{14} . For major disturbances, changing in T_{c1} and Q_{g2} were selected. So, from Eq.3.11.

$$\begin{bmatrix} \frac{\partial P_{2,op}}{\partial T_{c1}} & \frac{\partial m_{4,op}}{\partial T_{c1}} & \frac{\partial m_{14,op}}{\partial T_{c1}} \\ \frac{\partial P_{2,op}}{\partial Q_{g2}} & \frac{\partial m_{4,op}}{\partial Q_{g2}} & \frac{\partial m_{14,op}}{\partial Q_{g2}} \end{bmatrix} \begin{bmatrix} h_{P2} \\ h_{m4} \\ h_{m14} \end{bmatrix} = \begin{bmatrix} 0 \\ 0 \end{bmatrix} \quad (5.3)$$

There are many ways to estimate $\frac{\partial z_{op}}{\partial d}$. In this case, all $\frac{\partial z_{op}}{\partial T_{c1}}$ and $\frac{\partial z_{op}}{\partial Q_{g2}}$ values were represented by change in z_{op} when T_c increased by 2°C and Q_{g2} increased by 10% respectively.

$$\begin{bmatrix} -0.00238 & 4.108 & -4.948 \\ -0.00249 & 4.187 & -3.841 \end{bmatrix} \begin{bmatrix} h_{P2} \\ h_{m4} \\ h_{m14} \end{bmatrix} = \begin{bmatrix} 0 \\ 0 \end{bmatrix} \quad (5.4)$$

For $h_{P2} = 1$; $h_{m4} = 6.44E-4$ and $h_{m14} = 5.37E-5$ So, the final combined control variable from null space method was

$$P_2 + (6.44E - 4)m_4 + (5.37E - 5)m_{14} \quad ; \quad P_2 \text{ in MPa} \quad m_4 \text{ and } m_{14} \text{ in kg/min}$$

5.4 Location of Throughput Manipulator

The control structures were designed for two modes of operation; constant feed rate constant fixed production rate, so TPM was located at heat input and the cooling provided by an evaporator respectively. As mention before, both modes had significant differences in characteristic. In next chapter, the control structure in both modes were designed separately and the self-optimizing control variables were applied to the constant feed rate mode.

CHAPTER VI

BOTTOM-UP STRUCTURE DESIGN

The Bottom-up design of the control structure were explained in this chapter. To stabilize the system in regulatory control layer there were five levels, two pressures, one temperature and one production rate to be controlled.

Pressure and Temperature Control

Since the input-output pairs for pressure and temperature control were quite intuitive, they were the first to deal with. Since the streams leaving an absorber and both condensers were assumed to be saturated, it was logical to have the three pressures directly controlled by the heat utility input of those units. However, in case of a pressure in high-pressure cycle (P_2), its setpoint was set so that temperature in high-pressure generator is constant. The transfer functions for those input- output as well as all level control pairings, determined by step respond system identification, are listed in Appendix B.1.

6.1 On-Demand Mode of Operation

Level Control

As aforementioned, liquid level in this work was represented by liquid holdup in each unit. First thing to consider was level / holdup in an evaporator because it was a response of an integrating system. As there was no control valve and both inflow and outflow of the unit were not function of the liquid holdup, a system cannot re-stabilize itself to new steady state when face disturbance and would go unstable without proper control. This kind of system needs local consistence control i.e. it has to be controlled by a local manipulated variable. In this case heat utility of the evaporator was already used as production rate, so liquid holdup of an evaporator was controlled by a low-pressure condenser control valve. That left four holdup and four manipulated variables to be paired using RGA method. Those variables are shown in Table 6.1.

Table 6.1 input-output for liquid holdup control

Control variable	Manipulated variable
Mass in low-pressure condenser (M_{c1})	Heat input (Q_{g2})
Mass in high-pressure condenser (M_{c2})	High-pressure condenser control valve coefficient (Cm_{c2})
Mass in high-pressure generator (M_{g2})	High-pressure generator control valve coefficient (Cm_{g2})
Mass in low-pressure generator (M_{g1})	Low-pressure generator control valve coefficient (Cm_{g1})

The steady state gain for each pairing could be determined using transfer functions in Appendix B.1 and steady state RGA matrix was calculated as shown in Table.6.2. According to the RGA pairing rules, out of 24 possible pairs, only two were promising; control valve of both generators always controlled their own holdup and the pairing between heat input rate / high-pressure condenser control valve and holdup of both condensers could be interchangeable. Furthermore, since the two pairs seemed to have high level of interaction with each other, a MPC controller should also be suitable in this case and was designed as the third alternative. So, three control structures were proposed as shown in Fig.6.1 to Fig6.3. The tuning parameters for all PI and MPC controllers are shown in Appendix B.2.

Table 6.2 RGA values for liquid holdup control

	Q_{g2}	Cm_{c2}	Cm_{g2}	Cm_{g1}
M_{c1}	0.368	0.547	0.0389	0.046
M_{c2}	0.553	0.412	0.0316	0.00330
M_{g2}	0.0703	-0.0003	0.930	-0.00028
M_{g1}	0.00920	0.0408	-0.00078	0.951

Categories used to evaluate each control structure were dynamic disturbance sensitivity (DDS), maximum change in liquid holdup, overshoot of heat input, setting time and effect on LiBr mass fraction in stream entering an absorber (stream 6). Dynamic disturbance sensitivity (DDS) (Konda, 2005) can be described as an

alternative from of integral absolute error (IAE) as it uses the integral of absolute accumulation of all components as a measurement. And setting time in this work was defined as the interval where the level oscillation amplitude drops to less than 0.01%.

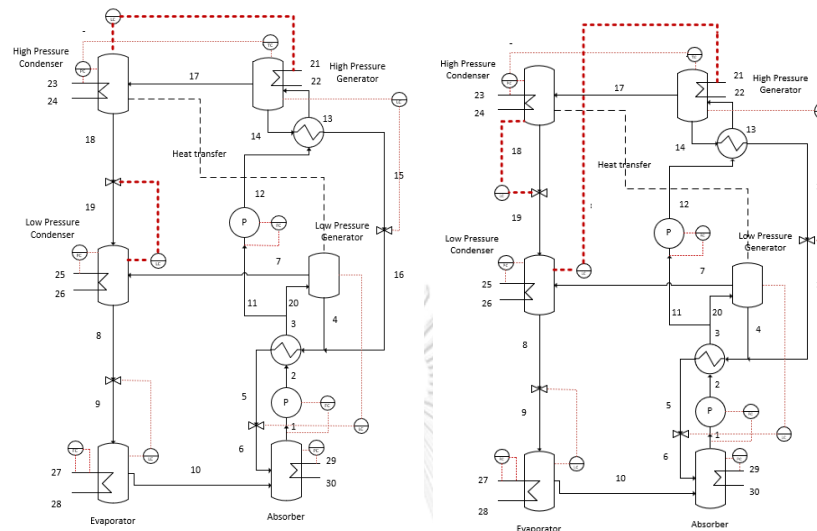


Figure 6.1 PID1 structure

Figure 6.2 PID2 structure

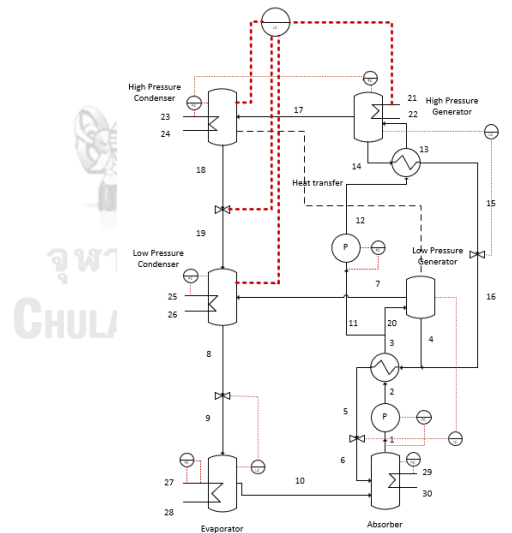


Figure 6.3 MPC structure

Figure 6.4 shows changes in level in the both condensers and heat input when cooling utility and low-pressure condenser temperature change by $\pm 2\%$ and, the DDS, change in liquid holdup, setting time and overshoot for each structure are shown in Table 6.3 and 6.4.

Table 6.3 Comparison of performance indices as T_{c1} decreased by 2°C

Tc-2	MPC	PID1	PID2
M_{c1} DDS (kg.min)	6.33	8.39	0.37
M_{c2} DDS (kg.min)	4.10	0.25	8.00
M_{c1} setting time (min)	31.66	34.87	9.28
M_{c2} setting time (min)	29.35	8.14	29.77
Max. change in M_{c1} (%)	1.55	1.89	0.17
Max. change in M_{c2} (%)	0.92	0.10	2.01
Q_{g2} Overshoot (kl/min)	878	744	841

As condenser temperature dropped from 32 to 30 °C, PID2 structure controlled M_{c1} better than others providing DDS equaled to 0.37 compared to 6.33 for MPC and 8.39 for PID1 structure. On the other hand, PID1 controlled M_{c2} better. The reason was level control using control valve was much more effective than heat input. As for total DDS, PID2 provided the least DDS at 8.37. It also provided the least setting time at 29.77 minute. Contrarily, the structure yielded the most change in liquid holdup.

Table 6.4 Comparison of performance indices as T_{c1} increased by 2°C

Tc+2	MPC	PID1	PID2
M_{c1} DDS (kg.min)	25.72	48.09	0.47
M_{c2} DDS (kg.min)	5.09	0.3	43.51
M_{c1} setting time (min)	69.85	80.86	13.63
M_{c2} setting time (min)	55.84	9.31	78.73
Max. change in M_{c1} (%)	1.84	2.18	0.19
Max. change in M_{c2} (%)	0.99	0.11	2.29
Q_{g2} Overshoot (kl/min)	0	0	0

As condenser temperature raised from 32 to 34 °C, MPC structure provided the least total DDS at 30.81 and the least setting time at 69.85 minute. Characteristic of the two PID structures was similar as their DDS are 48.39 and 43.98 and setting time were 80.86 and 78.73 minutes. Increasing in condenser temperature also raised LiBr mass fraction in stream entering an absorber however, in this case, there was no difference between each control structure as there was no overshoot in the LiBr mass fraction.

Control structure results as the cooling utility temperature changed

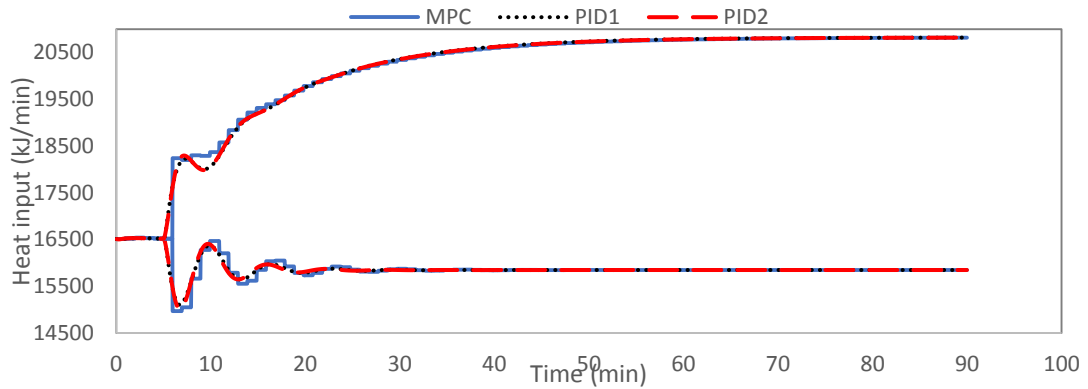


Figure 6.4a Heat input as T_{c1} changed by $\pm 2^\circ\text{C}$

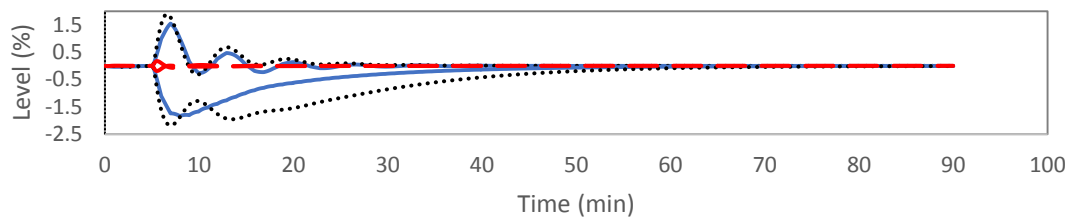


Figure 6.4b Level in C1 as T_{c1} changed by $\pm 2^\circ\text{C}$

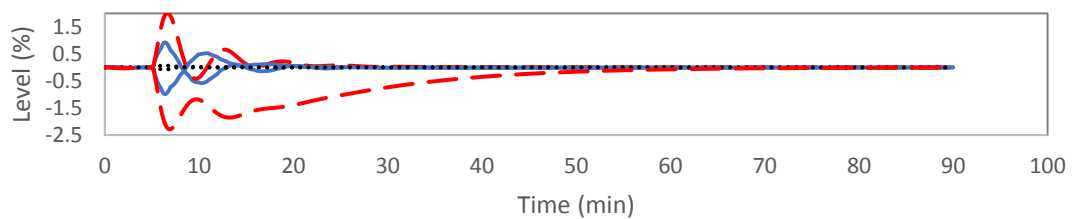


Figure 6.4c Level in C2 as T_{c1} changed by $\pm 2^\circ\text{C}$

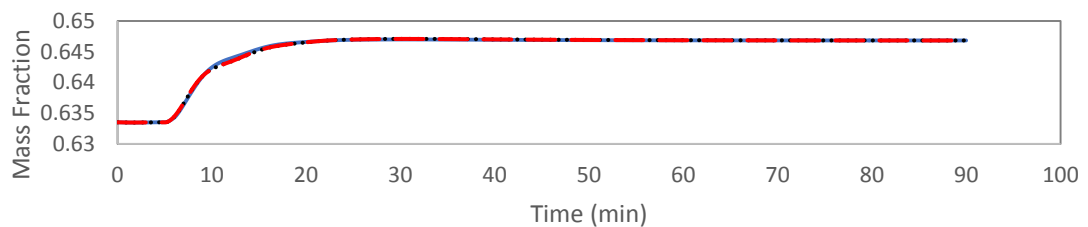


Figure 6.4d LiBr mass fraction as T_{c1} increased by 2°C

Simulation results for other cases of disturbance are shown in Table 6.5 – Table 6.7. In general, the results were similar with when condenser temperature changes as PID2 provided better results than PID1 in DDS and setting time categories but yielded a little bit more change in liquid holdup. As MPC and PID structures were compared, MPC provided significant better results in all categories in the cases that the change in disturbance caused increasing in heat input but performed slightly worse than PIDs as heat input was decreased, with the exception when production rate decreased. And for LiBr mass fraction, structures provided almost identical results as MPC controlled marginally better.

Table 6.5 Comparison of performance indices as production rate increased by 10%

TPM+10	MPC	PID1	PID2
M_{c1} DDS (kg.min)	25.77	48.26	0.7
M_{c2} DDS (kg.min)	8.57	0.27	43.66
M_{c1} setting time (min)	61.36	68.29	12.57
M_{c2} setting time (min)	48.25	9.34	66.16
Max. change in M_{c1} (%)	3.383	4.09	0.479
Max. change in M_{c2} (%)	1.706	0.081	4.53
Q_{g2} Overshoot (kJ/min)	0	0	0

Table 6.6 Comparison of performance indices as production rate decreased by 10%

TPM-10	MPC	PID1	PID2
M_{c1} DDS (kg.min)	14.33	21.25	0.82
M_{c2} DDS (kg.min)	4.20	0.29	19.23
M_{c1} setting time (min)	32.11	39.58	11.95
M_{c2} setting time (min)	32.29	8.62	34.81
Max. change in M_{c1} (%)	3.995	3.858	0.476
Max. change in M_{c2} (%)	0.754	0.097	4.337
Q_{g2} Overshoot (kJ/min)	1707	1039	1365

Table 6.7 Comparison of performance indices as T_e decreased by 2°C

Te-2	MPC	PID1	PID2
M_{c1} DDS (kg.min)	20.4	38.16	0.36
M_{c2} DDS (kg.min)	4.54	0.28	34.52
M_{c1} setting time (min)	56.83	76.33	12.19
M_{c2} setting time (min)	10.48	8.8	74.14
Max. change in M_{c1} (%)	1.282	1.716	0.128
Max. change in M_{c2} (%)	1.077	0.156	1.784
Q_{g2} Overshoot (kl/min)	0	0	0

Table 6.8 Comparison of performance indices as T_e increased by 2°C

Te+2	MPC	PID1	PID2
M_{c1} DDS (kg.min)	5.09	8.18	0.27
M_{c2} DDS (kg.min)	4.15	0.25	7.64
M_{c1} setting time (min)	28.72	34.84	8.74
M_{c2} setting time (min)	37.03	7.39	32.14
Max. change in M_{c1} (%)	1.182	1.674	0.129
Max. change in M_{c2} (%)	1.095	0.157	1.174
Q_{g2} Overshoot (kl/min)	820	547	604

Table 6.9 Comparison of performance indices as T_{g2} decreased by 5°C

Tg-5	MPC	PID1	PID2
M_{c1} DDS (kg.min)	10.84	22.22	0.21
M_{c2} DDS (kg.min)	4.13	0.23	20.4
M_{c1} setting time (min)	51.46	61.9	3.43
M_{c2} setting time (min)	39.40	5.77	59.5
Max. change in M_{c1} (%)	1.090	1.554	0.054
Max. change in M_{c2} (%)	1.257	0.131	1.55
Q_{g2} Overshoot (kl/min)	0	0	0

Table 6.10 Comparison of performance indices as T_{g2} increased by 5°C

Tg+5	MPC	PID1	PID2
M_{c1} DDS (kg.min)	4.80	8.27	0.25
M_{c2} DDS (kg.min)	4.48	0.29	7.84
M_{c1} setting time (min)	31.30	32.77	8.89
M_{c2} setting time (min)	31.75	7.87	30.76
Max. change in M_{c1} (%)	0.991	1.368	0.077
Max. change in M_{c2} (%)	1.391	0.19	1.391
Q_{g2} Overshoot (kl/min)	593	487	499



Control structure results as the production rate changed

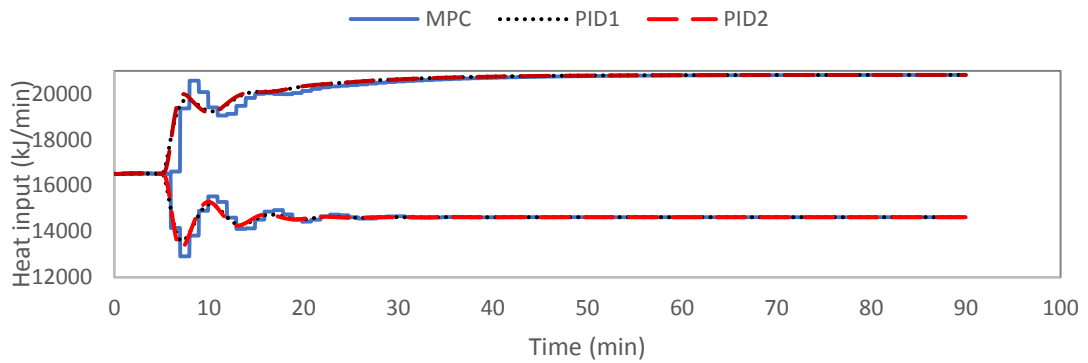


Figure 6.5a Heat input as production rate changed by $\pm 10\%$

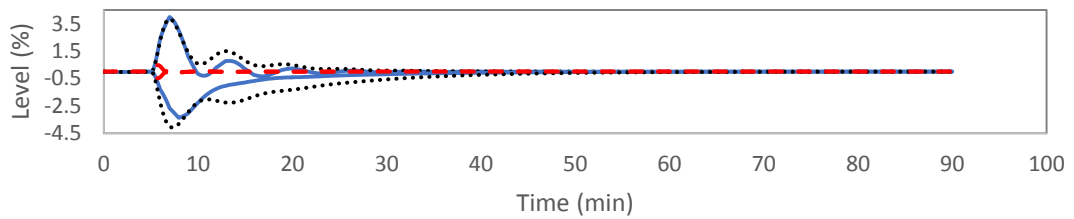


Figure 6.5b Level C1 in as production rate changed by $\pm 10\%$

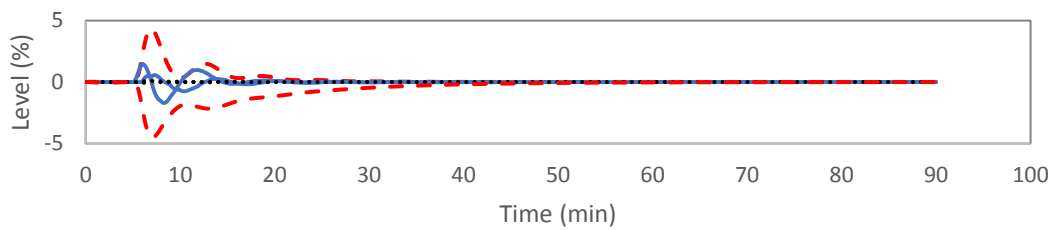


Figure 6.5c Level C2 in as production rate changed by $\pm 10\%$

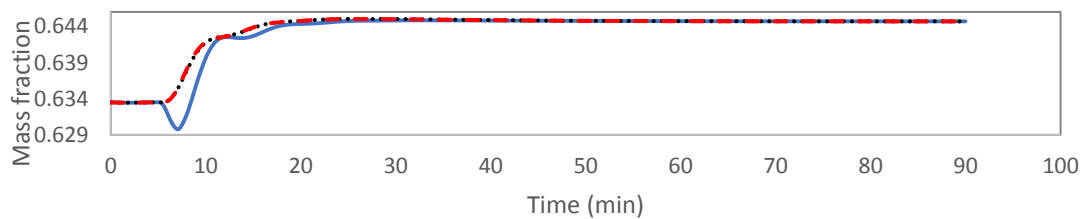


Figure 6.5d LiBr mass fraction as production rate increased by $\pm 10\%$

Control structure results as the desired temperature of chilled water changed

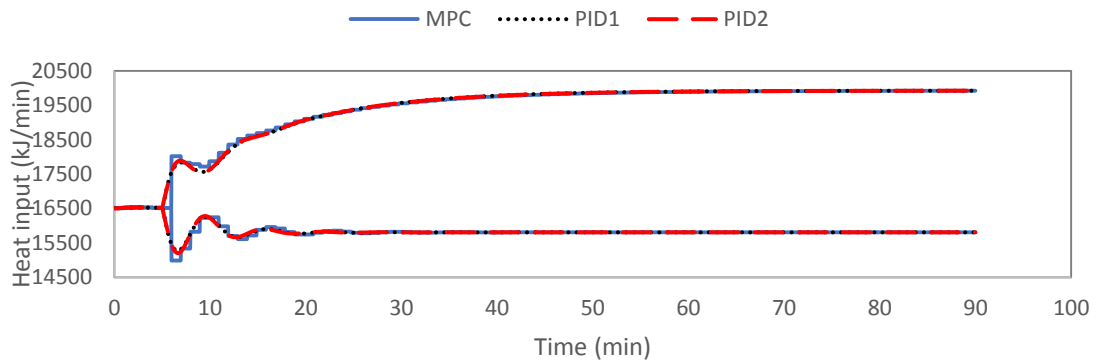


Figure 6.6a Heat input as T_e changed by $\pm 2^\circ\text{C}$

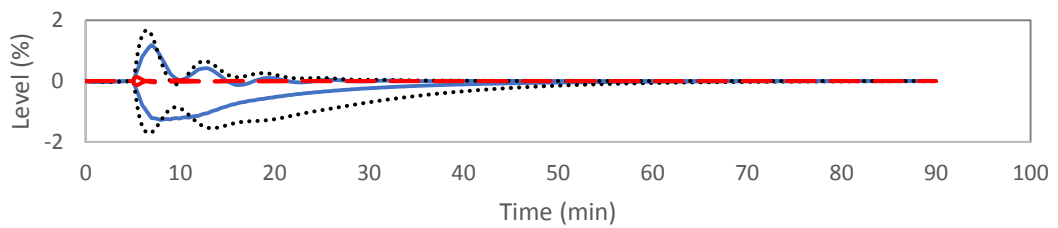


Figure 6.6b Level in C1 as T_e changed by $\pm 2^\circ\text{C}$

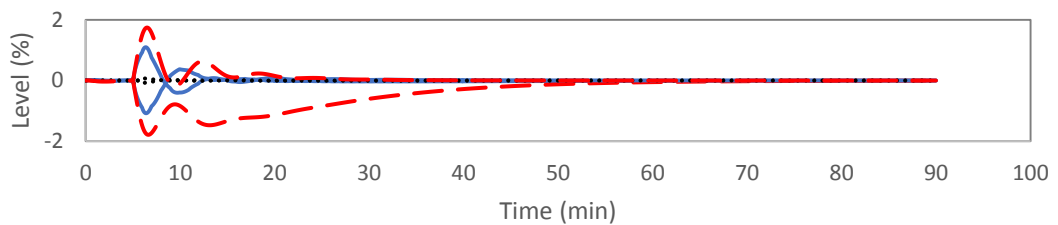


Figure 6.6c Level in C2 as T_e changed by $\pm 2^\circ\text{C}$

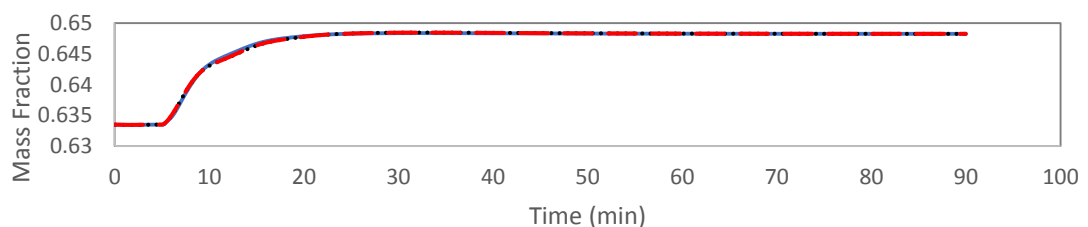


Figure 6.6d LiBr mass fraction T_e reduced by 2°C

Control structure results as temperature of heat input changed

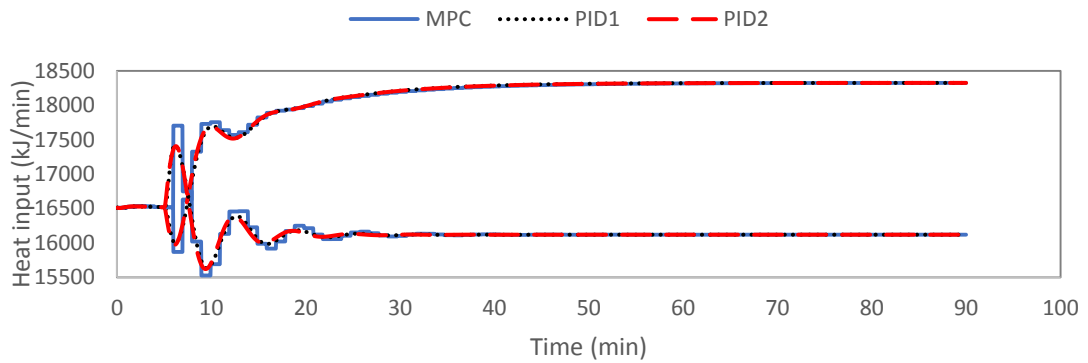


Figure 6.7a Heat input as T_{g2} changed by $\pm 5^\circ\text{C}$

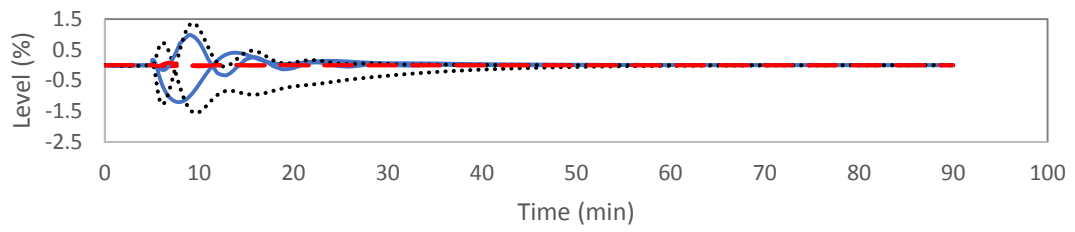


Figure 6.7b Level in C1 as T_{g2} changed by $\pm 5^\circ\text{C}$

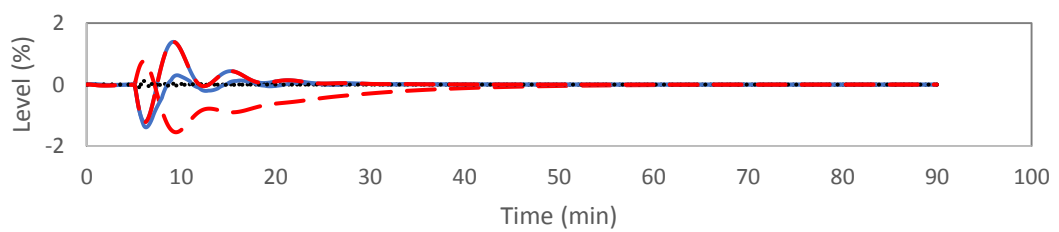


Figure 6.7c Level C2 in as T_{g2} changed by $\pm 5^\circ\text{C}$

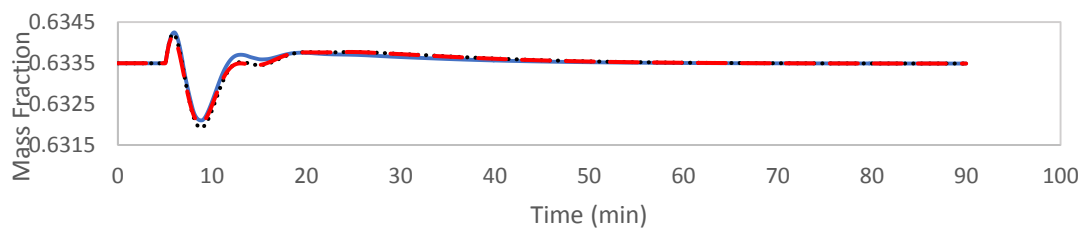


Figure 6.7d LiBr mass fraction as T_{g2} reduced by 5°C

Remark:1 Dynamic relative gain array (DRGA)

Although both PID structures shown almost identical results while deal with step change in disturbance, their responds to other types of disturbance are not necessary the same. So, DRGA analysis was performed to predicted controllability of the structure for each frequency. As shown in Fig.6.8 At low frequency, RGA ratio between PID 1 and PID 2 was around 6:4 so their controllability was about the same. But at high frequency, RGA of PID2 was almost unity whereas RGA of PID1 dropped to almost zero. It indicated that PID 2 should overall be the better structure.

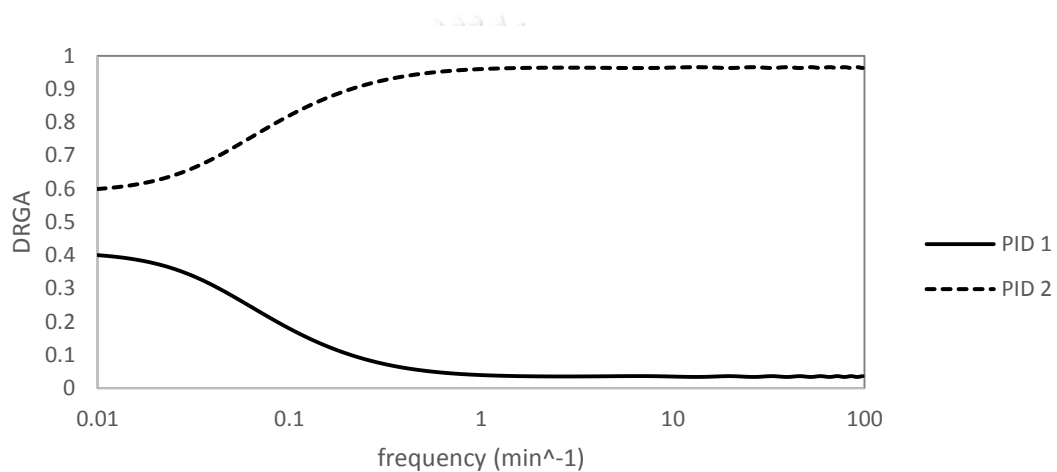


Figure 6.8 DRGA

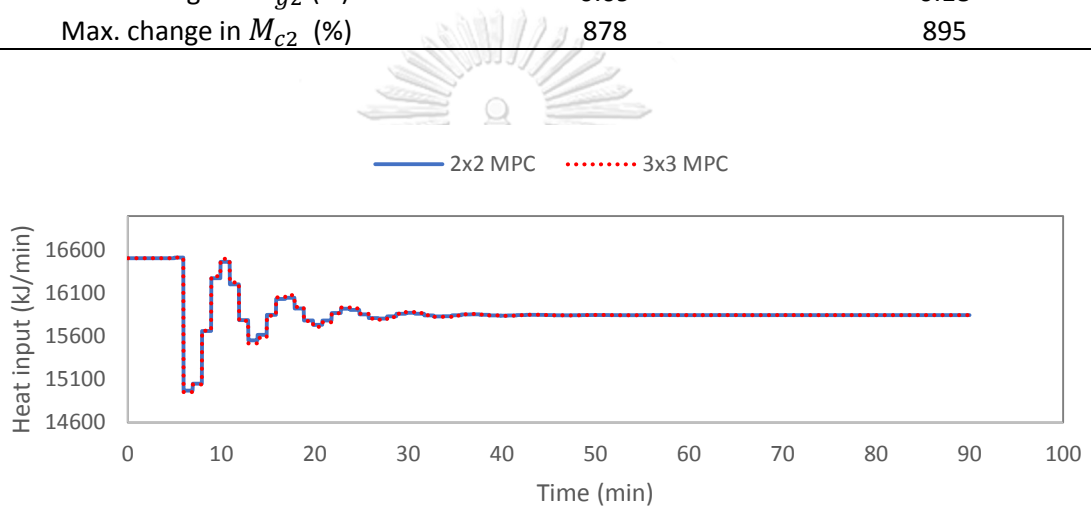
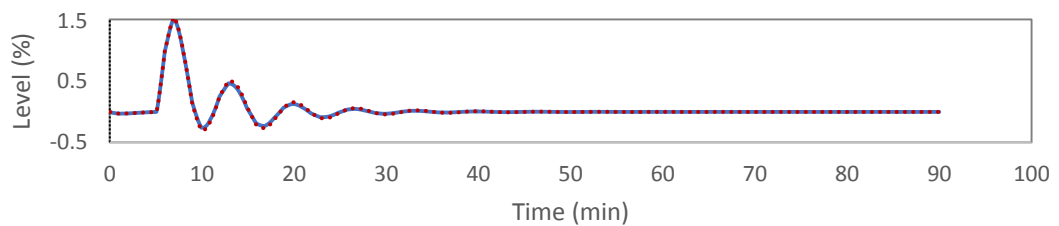
Remark:2 Three inputs – three outputs (3x3) MPC

The main reason that MPC was utilized is the high-degree of interaction between input and output pairs. There was not much benefit to add more input-output pairs with little interaction with the others to the controller. Table.6.11 shows a compared result of the 2x2 MPC structure shown previously and a 3x3 MPC structure with an addition pair of a high-pressure generator control valve and its level when a condenser temperature dropped by 2 °C.

Theoretically, with perfect process model and tuning, 3x3 MPC structure should provide marginal better results than 2x2 MPC. However, since model used for MPC was a linear approximation of the process, adding more variables led to more model mismatch. As shown in the table, 3x3 MPC performed slightly worse than 2x2 MPC structure in every category.

Table 6.11 MPC structure comparison as T_{c1} decreased by 2 °C

	2x2 MPC	3x3 MPC
M_{c1} DDS (kg.min)	6.33	6.79
M_{c2} DDS (kg.min)	4.10	4.47
M_{g2} DDS (kg.min)	0.42	0.8349
M_{c1} setting time (min)	31.66	35.23
M_{c2} setting time (min)	29.35	29.80
M_{g2} setting time (min)	12.94	16.24
Max. change in M_{c1} (%)	1.55	1.56
Max. change in M_{c2} (%)	0.92	0.95
Max. change in M_{g2} (%)	0.09	0.18
Max. change in M_{c2} (%)	878	895

**Figure 6.9a** Heat input as T_{c1} decreased by 2°C**Figure 6.9b** Level in C2 as T_{c1} decreased by 2°C

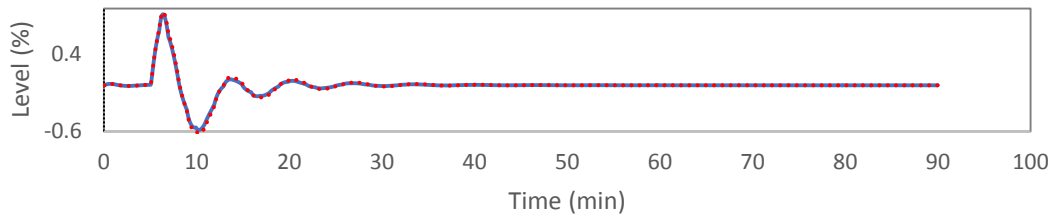


Figure 6.9c Level in C1 as T_{c1} decreases by 2°C

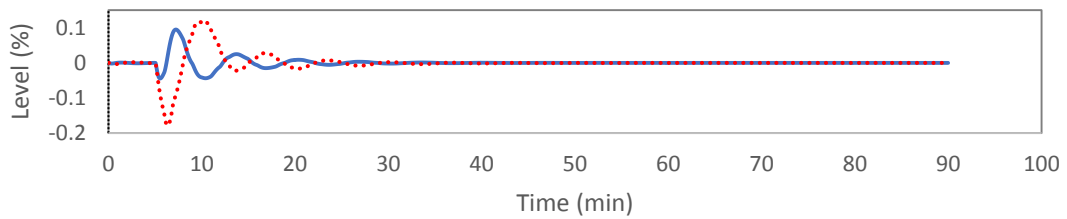


Figure 6.9d Level in G2 as T_{c1} decreased by 2°C

6.2 On-Supply Mode of Operation

In this mode, the liquid holdup in an evaporator was controlled by flow rate of chilled water. So, that left a low-pressure condenser control valve as the 4th manipulated variable instead of heat input. Table 6.12 shows RGA matrix for this case.

Table 6.12 RGA values for liquid holdup control in on-supply mode

	Cm_{c2}	Cm_{c1}	Cm_{g2}	Cm_{g1}
M_{c1}	0.0110	0.991	0.00737	-0.0102
M_{c2}	0.988	0.00316	0.00648	0.00233
M_{g2}	0.000988	0.0123	0.987	-0.00073
M_{g1}	2.25E-06	-0.00723	-0.00133	1.01

From the table, it was apparent that there was only one promising control structure with each control valve controlled liquid holdup of their own unit as shown in Figure 6.10. For the supervisory control, both pressure in the high-pressure cycle (P_2) and the combined measurement from null space method ($P_2 + (6.44E - 4)m_4 +$

$(5.37E - 5)m_{14}$) were used as the self-optimizing control variables to improve process COP.

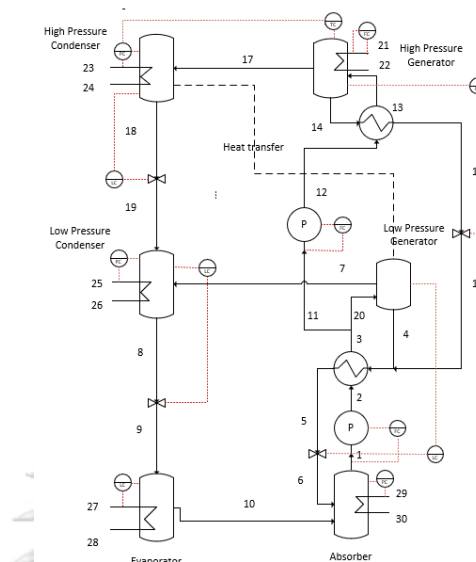


Figure 6.10 PID 3 structure

Figure 6.11. shows effects of the self-optimizing control variables on COP and its corresponding splitting ratio when a low-pressure condenser temperature changed by $\pm 2^\circ\text{C}$. There was a clear difference between structures with a self-optimizing and a structure with constant splitting ratio as the final results were about the same as estimated by a steady state simulation (94.76 and 51.50% loss reduction in case of P_2). Moreover, effects on dynamic of the process was negligible as their setting time and overshoot are about the same. When comparing between P_2 and the combined measurement, the latter provides a little more COP as the combined measurement structure's COP were 1.2150 and 1.3887 whereas P_2 structure gives 1.2137 and 1.3866 for the case that a low-pressure condenser temperature increases and decreases by 2°C respectively.

Figure 6.11 - Figure 6.14 shows the effects of the self-optimizing control variables as well as the change in splitting ratio which was the manipulated variable in other cases of disturbance. The results were the same in case that the amount of heat input to the system changes as the combined measurement provides slightly higher COP than P_2 . However, it provided a little less COP in a case that evaporator

temperature is decreased. Improvement in COP was not guarantee in this case because the change in evaporator temperature was not the main disturbance used when calculated the combined measurement.

Also, in the case that temperature of heat input changed, due to high correlation between the temperature and P_2 , both self-optimizing structures made the dynamic of the process worse as reflected in higher overshoot in COP which also represents the production rate. And in the case that the temperature dropped, the combined variable yielded even less COP than the structure with constant ratio. The comparison of COP for each structure are shown Table 6.13

Table 6.13 COP at the worst cases of disturbance

	No CV	P_2	Combined variable
$T_{c1}+2^\circ\text{C}$	1.1880	1.2137	1.2150
$T_{c1}-2^\circ\text{C}$	1.3730	1.3859	1.3888
$Q_{g2}-10\%$	1.3369	1.3509	1.3542
$Q_{g2}+10\%$	1.2488	1.2706	1.2720
$T_e-2^\circ\text{C}$	1.2196	1.2429	1.2417
$T_e+2^\circ\text{C}$	1.3767	1.3895	1.3915
$T_{g2}+5^\circ\text{C}$	1.3475	1.3607	1.3608
$T_{g2}-5^\circ\text{C}$	1.2710	1.2887	1.2700

Self-optimizing variable results as the cooling utility temperature changed

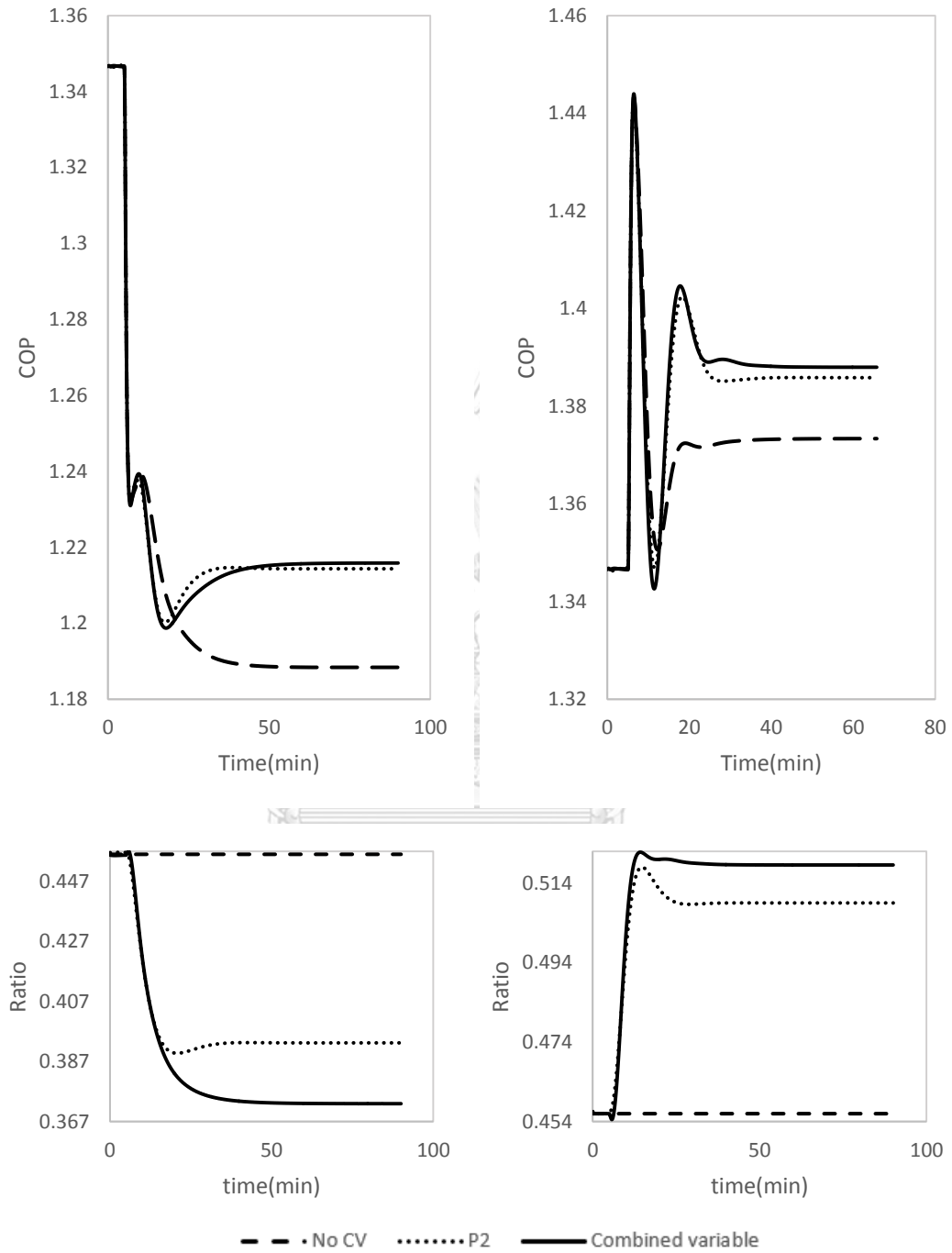


Figure 6.11 COP for each structure as T_{c1} increased by 2°C (left) and decreased by 2°C (right)

Self-optimizing variable results as the amount of heat input to the system changed

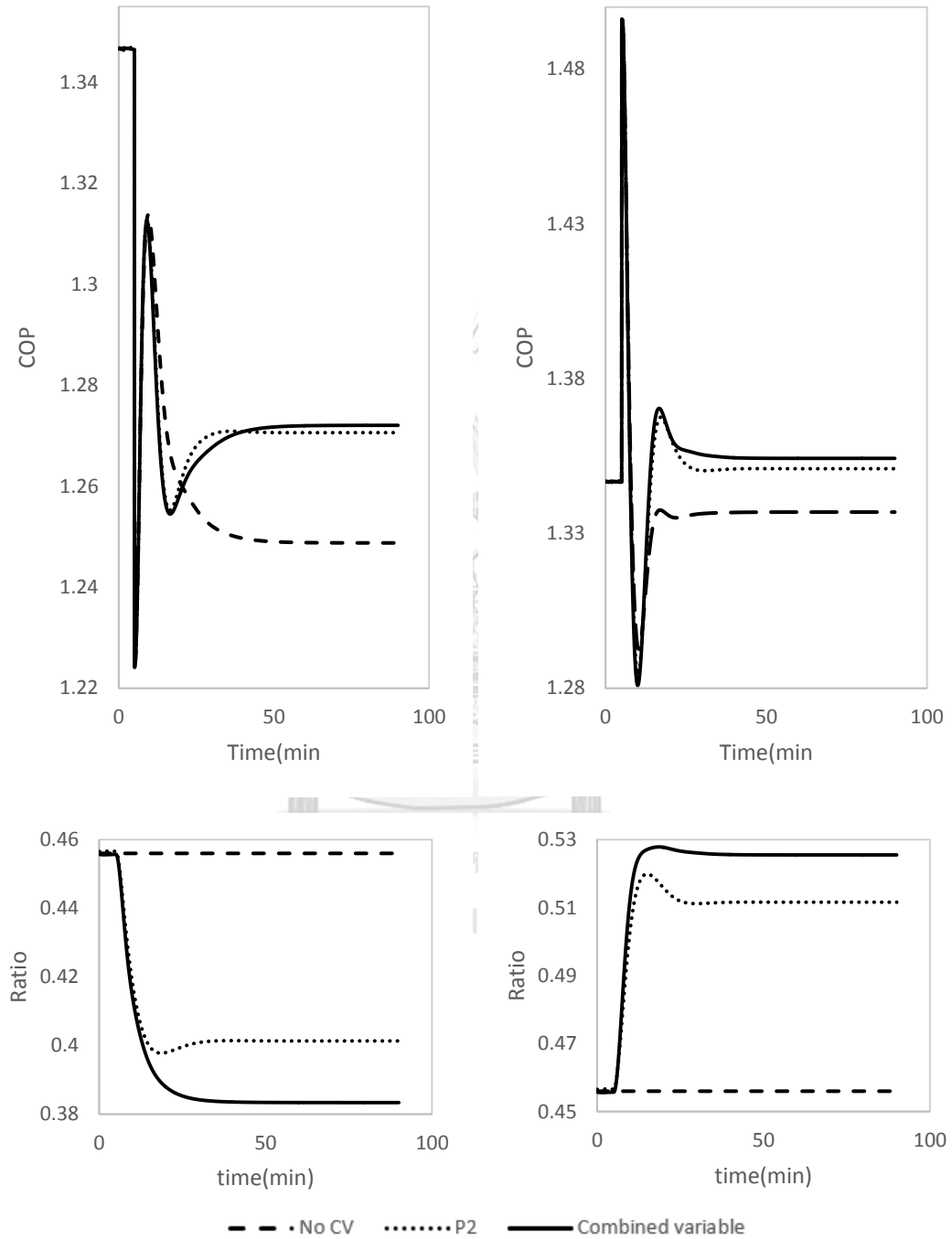


Figure 6.12 COP for each structure as Q_{g2} increased by 10% (left) and decreased by 10% (right)

Self-optimizing variable results as the desired temperature of chilled water changed

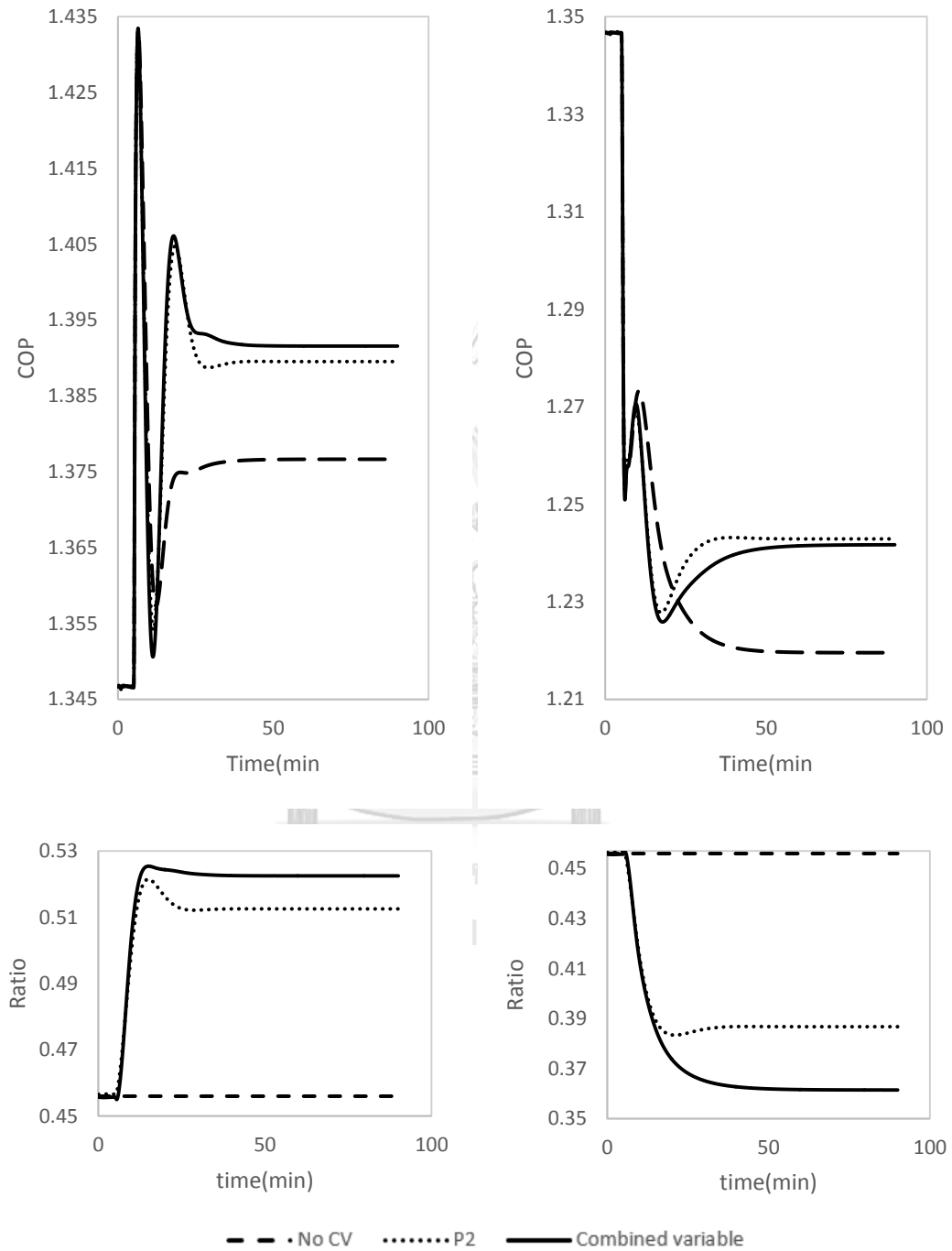


Figure 6.13 COP for each structure as T_e increased by 2°C (left) and decreased by 2°C (right)

Self-optimizing variable results as temperature of heat input changed

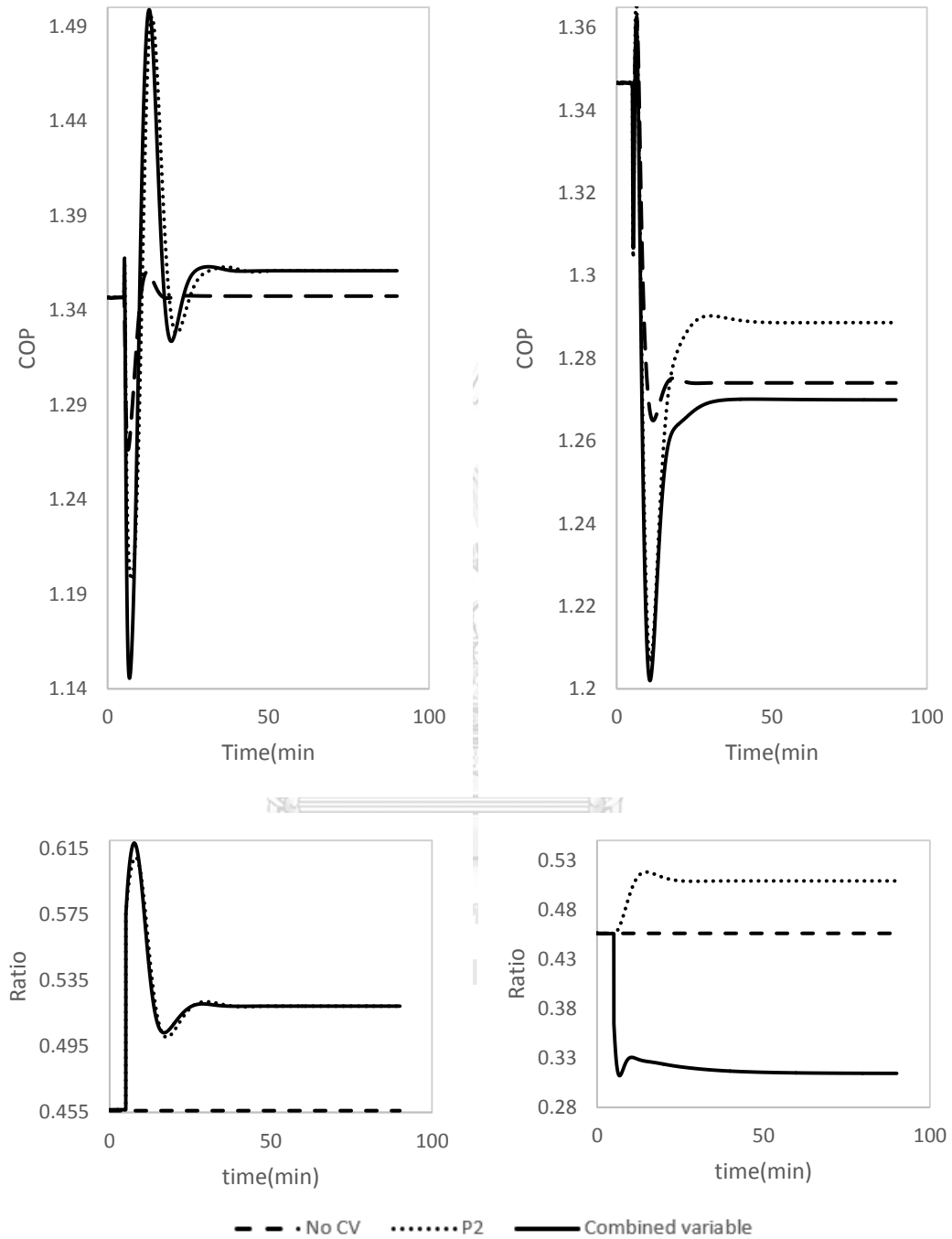


Figure 6.14 COP for each structure as T_{g2} increased by 5°C (left) and decreased by 5°C (right)

CHAPTER VII

CONCLUSIONS

In this study, Skogstad's plantwide control procedure was applied to a parallel flow double effect water/lithium bromide absorption chiller operated in two modes; on-demand and on-supply.

1. For on-demand mode, as two decentralized structures were compared, the structure using heat input to control liquid holdup in a high-pressure condenser provided slightly better result in most scenarios.
2. When decentralized structures were compared with a MPC structure, the latter performed better in the cases that the disturbance caused increasing in heat input but performed slightly worse than the decentralized structures in cases that heat input is decreased.
3. For on-supply mode, two self-optimizing control variables were applied to the process. both pressure in high-pressure cycle and combined measurement from null space method perform well and could reduce loss due to change in optimal process conditions around 50 – 99%. However, since the results were similar, it might be better to use the pressure as the self-optimizing control variable because of its simplicity.
4. On the other hand, as temperature of the heat source changed, both self-optimizing structures had the negative impact on dynamic behavior of the process.

Recommendation

In this work, the process only has one free degree of freedom. To further evaluate effects of self-optimizing control, applying the method to more complex processes is encouraged.

REFERENCES

- ASHRAE handbook: Fundamentals*. (2009). Atlanta: American Society of Heating, Refrigerating and Air-Conditioning Engineers.
- Berestneff, A. A. (1949). Control arrangement for absorption refrigeration systems. In: Google Patents.
- Buckley, P. S. (1964). Techniques for process control.
- Dixit, M. (2016). *Energy and Exergy Analysis of a Double Effect Parallel Flow LiBr/H₂O Absorption Refrigeration System* (Vol. 2).
- Fernández-Seara, J., & Vázquez, M. (2001). Study and control of the optimal generation temperature in NH₃-H₂O absorption refrigeration systems. *Applied Thermal Engineering*, 21(3), 343-357.
- Foss, A. S. (1973). Critique of chemical process control theory. 19(2), 209-214.
- Gilani, S. I., & Ahmed, M. S. M. S. (2015). Solution Crystallization Detection for Double-effect LiBr-H₂O Steam Absorption Chiller. *Energy Procedia*, 75, 1522-1528.
- Govind, R., & Powers, G. J. (1982). Control system synthesis strategies. 28(1), 60-73. doi:doi:10.1002/aic.690280110
- Grosdidier, P., Morari, M., & Holt, B. R. (1985). Closed-loop properties from steady-state gain information. *Industrial & Engineering Chemistry Fundamentals*, 24(2), 221-235.
- Halvorsen, I. J., Skogestad, S., Morud, J. C., & Alstad, V. (2003). Optimal Selection of Controlled Variables. *Industrial & Engineering Chemistry Research*, 42(14), 3273-3284.
- Herold, K. E., Radermache, R., & Klein, S. A. (2016). Absorption Chillers and Heat Pumps. 2.
- Jeong, S., Kang, B. H., & Karng, S. W. (1998). Dynamic simulation of an absorption heat pump for recovering low grade waste heat. *Applied Thermal Engineering*, 18(1), 1-12.
- Khan, M. M. A., Saidur, R., & Al-Sulaiman, F. A. (2017). A review for phase change materials (PCMs) in solar absorption refrigeration systems. *Renewable and Sustainable Energy Reviews*, 76, 105-137.
- Kohlenbach, P., & Ziegler, F. (2008). *A dynamic simulation model for transient absorption chiller performance. Part I: The model* (Vol. 31).

- Konda, N. V. S. N., Rangaiah, G. P., & Krishnaswamy, P. R. (2005). Plantwide Control of Industrial Processes: An Integrated Framework of Simulation and Heuristics. *Industrial & Engineering Chemistry Research*, 44(22), 8300-8313.
- Larsson, T., & Skogestad, S. (2000). *Plantwide control - A review and a new design procedure* (Vol. 21).
- Lazrak, A., Boudehenn, F., Bonnot, S., Fraisse, G., Leconte, A., Papillon, P., & Souyri, B. (2016). Development of a dynamic artificial neural network model of an absorption chiller and its experimental validation. *Renewable Energy*, 86, 1009-1022.
- Li, Z. F., & Sumathy, K. (2000). Technology development in the solar absorption air-conditioning systems. *Renewable and Sustainable Energy Reviews*, 4(3), 267-293.
- Luyben, M. L., Tyreus, B. D., & Luyben, W. L. (1997). Plantwide control design procedure. 43(12), 3161-3174.
- McAvoy, T. J. (1983). Some results on dynamic interaction analysis of complex control systems. *Industrial & Engineering Chemistry Process Design and Development*, 22(1), 42-49.
- McAvoy, T. J., & Ye, N. (1994). Base control for the Tennessee Eastman problem. *Computers & Chemical Engineering*, 18(5), 383-413.
- Morari, M., Arkun, Y., & Stephanopoulos, G. (1980). Studies in the synthesis of control structures for chemical processes: Part I: Formulation of the problem. Process decomposition and the classification of the control tasks. Analysis of the optimizing control structures. 26(2), 220-232.
- Narraway, L., & Perkins, J. (1993). *Selection of Process Control Structure Based on Linear Dynamic Economics* (Vol. 32).
- Rangaiah, G. P., & Kariwala, V. (2012). *Plantwide control: Recent developments and applications*: John Wiley & Sons.
- Rêgo, A. T., Hanriot, S. M., Oliveira, A. F., Brito, P., & Rêgo, T. F. U. (2014). Automotive exhaust gas flow control for an ammonia–water absorption refrigeration system. *Applied Thermal Engineering*, 64(1), 101-107.
- Seborg, D. E., Mellichamp, D. A., Edgar, T. F., & Doyle III, F. J. (2010). *Process dynamics and control*: John Wiley & Sons.
- Seo, J. A., Shin, Y., & Chung, J. D. (2012). Dynamics and control of solution levels in a high temperature generator for an absorption chiller. *International Journal of*

- Refrigeration*, 35(4), 1123-1129.
- Shin, Y., Seo, J. A., Cho, H. W., Nam, S. C., & Jeong, J. H. (2009). Simulation of dynamics and control of a double-effect LiBr–H₂O absorption chiller. *Applied Thermal Engineering*, 29(13), 2718-2725.
- Skogestad, S. (2000). Plantwide control: The search for the self-optimizing control structure. *10*(5), 487-507.
- Skogestad, S. (2004). Control structure design for complete chemical plants. *28*(1-2), 219-234.
- Skogestad, S., & Postlethwaite, I. (1996). Multivariable Feedback Control: Analysis and Design. In.
- Smith, J. M., Van Ness, H. C., & Abbott, M. M. (2005). Introduction to Chemical Engineering Thermodynamics.
- Stephanopoulos, G. (1983). Synthesis of control systems for chemical plants A challenge for creativity. *7*(4), 331-365.
- Wolff, E., Perkins, J., & Skogestad, S. (1994). *Procedure for operability analysis*.
- Wongsri, M., & Arpornwichanop, A. (2006). *Design of plantwide control structure*.
- Xu, Y.-j., Zhang, S.-j., & Xiao, Y.-h. J. A. T. E. (2016). Modeling the dynamic simulation and control of a single effect LiBr–H₂O absorption chiller. *107*, 1183-1191.
- Zhang, C., Vasudevan, S., & Rangaiah, G. (2010). *Plantwide Control System Design and Performance Evaluation for Ammonia Synthesis Process* (Vol. 49).
- Zheng, A., Mahajanam, R. V., & Douglas, J. M. J. A. J. (1999). Hierarchical procedure for plantwide control system synthesis. *45*(6), 1255-1265.

APPENDIX

A.1 System Identification

In order to calculate the RGA matrix and proper tuning PI controllers, the first-order with time delay transfer function of the input-output pairs, $\frac{k}{\tau s + 1} \exp(-\theta s)$, are required. In practice, a transfer function can be easily obtained by step response experiment as k is determined by ratio between Δu and $\Delta y(\infty)$, θ is the time delay before y starts to change and τ is the time y takes to reach 63 % of the $\Delta y(\infty)$

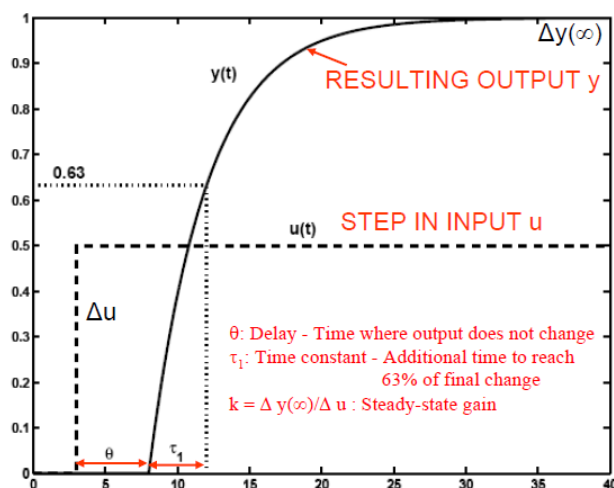


Figure A.1 step response experiment (Skogastad, 2012)

On the other hand, the transfer functions can also be derived from the mathematic model directly. The first-order with time delay transfer function can be estimated from detailed high-order model; $\frac{\prod_j(-T_j s + 1)}{\prod_i(\tau_i s + 1)} \exp(-\theta_0 s)$ where $\tau_1 \geq \tau_2 \geq \dots \geq \tau_n$ by Skogastad's half rule model reduction as

$$\tau = \tau_1 + \frac{\tau_2}{2} \tag{A.1}$$

$$\theta = \theta_0 + \frac{\tau_2}{2} + \sum_{i \geq 3} \tau_i + \sum_j T_j \tag{A.2}$$

A.2 PI Controller Tuning

After the transfer function acquired, the most common way to determine controller parameters is the Ziegles-Nichols setting (1942). For PI controller. The closed loop step test respond with a P controller is performed to obtain the ultimate gain (K_u) and ultimate period (P_u). As the ultimate gain is defined as the gain that the closed loop respond has sustained oscillations and ultimate period is the period of the sustained oscillations. For a PI controller, its parameters can be calculated as

$$K_p = \frac{K_u}{2.2} \quad (\text{A.3})$$

$$\tau_i = \frac{P_u}{1.2} \quad (\text{A.4})$$

The downsides of Ziegles-Nichols are it provides rather aggressive response and it gives poor performance for process with a dominant delay (Skogastad, 2012). Skogastad also included his PI tuning method in his procedure. In his method, PI parameters can be calculated as

$$K_p = \frac{1}{k} \frac{\tau}{\tau_c + \theta} \quad (\text{A.5})$$

$$\tau_i = \min\{\tau, 4(\tau_c + \theta)\} \quad (\text{A.6})$$

As τ_c is a desired first-order closed-loop time constant. In this work, MATLAB-Simulink was used to estimate the closed-loop response directly from the transfer function. And to compare performance between different structure, τ_c of each SISO closed-loop was set to be about the same.

B.1 Transfer Functions

Transfer functions obtained by step response experiment at an absorption chiller nominal operating conditions are listed as follows

$$\Delta P_0 = \frac{5.367e - 7}{s + 1.228} \exp(-0.78s) \Delta Q_a$$

$$\Delta P_1 = \frac{-3.316e - 7}{s + 0.07533} \Delta Q_{c1}$$

$$\Delta P_2 = \frac{-4.109e - 6}{s + 0.07411} \Delta Q_{c2}$$

Table B.1.1 Transfer functions for liquid holdup control

	M_{c1}	M_{c2}	M_{g1}	M_{g2}
M_{c1}	$\frac{-5.936}{s + 0.1654}$	$\frac{0.03772}{s + 0.03696}$	$\frac{6.857}{s + 0.6169}$	$\frac{1.638e - 5}{s + 0.02757} \exp(-0.18s)$
M_{c2}	$\frac{-0.2635s - 0.005127}{s^2 + 0.1394s + 0.008886}$	$\frac{-0.3797}{s + 0.2995} \exp(-0.87s)$	$\frac{-5.831}{s + 0.09618}$	$\frac{0.0003956}{s + 0.08493} \exp(-0.66s)$
M_{g1}	$\frac{3.228}{s + 0.2486}$	$\frac{2.92}{s + 0.09565} \exp(-0.87s)$	$\frac{0.05213}{s + 0.1085}$	$\frac{5.354e - 5}{s + 0.06297} \exp(-0.87s)$
M_{g2}	$\frac{3.441}{s + 0.1453}$	$\frac{1.569}{s + 1.131} \exp(-0.06s)$	$\frac{-5.916}{s + 0.1297}$	$\frac{-0.0004418}{s + 0.07308} \exp(-0.75s)$

B.2 Controller Parameters

Table B.2.1 PI Controller parameters

Structure	Controlled variables	Manipulate Variables	Action	Tuning parameter	
				Kp	τ
PID 1	M_{g1}	CmG1	Reverse	0.2274	0.9765
	M_{g2}	CmG2	Reverse	0.2125	1.063
	P_2	Q_{c2}	Reverse	9936	0.3518
	P_1	Q_{c1}	Reverse	1.08E+05	0.3328
	P_0	Q_a	Reverse	3.03E+05	1.516
PID 2	M_{c1}	Q_{g2}	Direct	439.7	0.06689
	M_{c2}	Cm_{c2}	Reverse	0.4023	3.4230
	M_e	Cm_{c1}	Direct	0.5589	2.297
PID 3	M_{c1}	Cm_{c2}	Direct	0.7186	2.774
	M_{c2}	Q_{g2}	Direct	491.1	0.06530
	M_e	Cm_{c1}	Direct	0.5589	2.297
	M_{c1}	Cm_{c1}	Reverse	0.4654	1.952
	M_{c2}	Cm_{c2}	Reverse	0.4023	3.4230
	M_e	Q_e	Direct	6938	1.854
	P_2	R	Reverse	9.212	0.2573
	Combined variable	R	Reverse	8.016	0.1517

Table B.2.2 MPC Controller parameters

MPC	Controlled variables	Manipulate Variables	Prediction horizon	Control horizon	Sample time
	M_{c1}, M_{c2}	Cm_{c2}, Q_{g2}	120	12	1 minute
Weight	Q_{g2}	CmC2		M_{c1}	M_{c2}
Rate	0.1	0		1	1
Weight	0.1	0.0001		0	0

VITA

NAME Kris Prasopsanti
DATE OF BIRTH 19 July 1990
PLACE OF BIRTH Bangkok
**INSTITUTIONS
ATTENDED** Chulalongkorn University
HOME ADDRESS 239/25 Lumpini Pathumwan Bangkok 10330



จุฬาลงกรณ์มหาวิทยาลัย
CHULALONGKORN UNIVERSITY